Anthropogenic climate change will intensify European explosive storms similar to Alex, Eunice, and Xynthia in the future

Mireia Ginesta, Emmanouil Flaounas, Pascal Yiou, Davide Faranda

▶ **To cite this version:**

Mireia Ginesta, Emmanouil Flaounas, Pascal Yiou, Davide Faranda. Anthropogenic climate change will intensify European explosive storms similar to Alex, Eunice, and Xynthia in the future. 2024. hal-04477289v2

HAL Id: hal-04477289
https://hal.science/hal-04477289v2

Preprint submitted on 25 Jun 2024

HAL is a multi-disciplinary open access archive for the deposit and dissemination of scientific research documents, whether they are published or not. The documents may come from teaching and research institutions in France or abroad, or from public or private research centers.

L'archive ouverte pluridisciplinaire **HAL**, est destinée au dépôt et à la diffusion de documents scientifiques de niveau recherche, publiés ou non, émanant des établissements d'enseignement et de recherche français ou étrangers, des laboratoires publics ou privés.

Anthropogenic climate change will intensify European explosive storms analogous to Alex, Eunice, and Xynthia

Mireia Ginesta,[a] Emmanouil Flaounas,[b] Pascal Yiou,[a] Davide Faranda,[a,c,d]

[a] *Laboratoire des Sciences du Climat et de l'Environnement, UMR 8212 CEA-CNRS-UVSQ, Univ. Paris-Saclay & IPSL, Orme des Merisiers, 91191 Gif-sur-Yvette, France*

[b] *Institute of Oceanography, Hellenic Center for Marine Research, Athens, Greece*

[c] *London Mathematical Laboratory, 8 Margravine Gardens, London, W6 8RH, UK*

[d] *LMD/IPSL, Ecole Normale Supérieure, PSL research University, 75005, Paris, France*

Corresponding author: Mireia Ginesta, Mireia.Ginesta-Fernandez@lsce.ipsl.fr

ABSTRACT: Extratropical storms, particularly explosive storms or 'weather bombs' with exceptionally high deepening rates, present substantial risks and are susceptible to climate change. Individual storms may exhibit a complex and hardly detectable response to human-driven climate change because of the atmosphere's chaotic nature and variability at regional level. It is thus essential to understand changes in specific storms for building local resilience and advancing our overall comprehension of storm trends. To address this challenge, this study compares analogues – storms with a similar backward track until making landfall — in two climates of three explosive storms impacting different European locations: Alex (October 2020), Eunice (January 2022), and Xynthia (February 2010). We use a large ensemble dataset of 105 members from the Community Earth System Model version 1 (CESM1). These analogues are identified in two periods: the present-day climate (1991-2001) and a future climate scenario characterized by high anthropogenic greenhouse gas emissions (RCP8.5, 2091-2101).

We evaluate future changes in the frequency of occurrence of the storms and intensity, as well as on meteorological hazards and the underlying dynamics. For all storms, our analysis reveals an increase in precipitation and wind severity over land associated with the explosive analogues in the future climate. These findings underscore the potential consequences of explosive storms modified by climate change and their subsequent hazards on various regions of Europe, offering evidence that can be used to prepare and enhance adaptation processes.

SIGNIFICANCE STATEMENT: This study investigates the impact of climate change on explosive storms, or 'weather bombs,' and their potential consequences for European regions. We project future scenarios of three specific storms, Alex, Eunice, and Xynthia, using a state-of-the-art climate model. Our findings reveal an increase in precipitation and wind over land associated to these storms, emphasizing the heightened risks associated with climate change. The significance lies in understanding the local implications of explosive storms, aiding in the development of resilient strategies and adaptation measures.

1. Introduction

Weather variability in the mid-latitudes is mainly controlled by atmospheric wave activity, consisting of propagating synoptic-scale cyclonic and anticyclonic circulation. Therein, extratropical storms play a key role in affecting the wave guide and producing the majority of high impact weather (Wallace and Hobbs 2006). They contribute substantially to total precipitation (Hawcroft et al. 2012) and are a source of wind energy (Liu et al. 2008; Rapella et al. 2023). Extratropical storms can also exhibit extreme behaviour, being associated with strong precipitation and flooding events (Hawcroft et al. 2018), strong and damaging winds (Roberts et al. 2014a), or a combination of both (Owen et al. 2021). Given their potential to be associated with meteorological hazards with significant socio-economic impacts (e.g., Liberato 2014; Jansa et al. 2001), understanding the evolution of their characteristics in a future climate is crucial.

Several studies have assessed the role of climate change in modifying the underlying dynamics of extratropical storms (e.g. Lehmann et al. 2014; Priestley and Catto 2022). Changes in frequency, position and intensity of the storm tracks, namely the preferred regions where storms travel through, are primary driven by changes in the horizontal temperature gradient in both lower and upper troposhere and in the vertical temperature profile (Catto et al. 2019). The Coupled Model Intercomparision Project (CMIP) phases 3, 5, and 6 generally agree on the spatial signature of the projected changes in storminess in the North Atlantic (Harvey et al. 2020). Specifically, models project a decrease in storm activity during summer, particularly in the southern regions, and produce a tripolar pattern in winter of an increase in storm activity in the British Isles and a decrease in the Mediterranean and Norwegian seas (Zappa et al. 2013; Priestley et al. 2020). Regarding extreme storms, the response consist of a decrease in frequency of ocurrence in the North

Atlantic basin, with a weak and local increase over the British Isles and the North Sea in winter (Zappa et al. 2013; Seiler and Zwiers 2016). Sources of uncertainty of climate projections stem from difficulties of isolating internal variability from the forced signal (Deser et al. 2012), as well scenario and model uncertainty (Hawkins and Sutton 2009; Sansom et al. 2013). In addition, low confidence still persists due to opposing thermodynamic processes that alter baroclinicity (Shaw et al. 2016), and challenges in resolving meso-scale and small scale features such as the diabatic processes (Schemm 2023).

While examining general trends in storm behaviour provides a fundamental understanding of the potential hazards of climate change, it is essential to recognize that specific storms may exhibit unique characteristics. This stems from the fact that specific storms are influenced by a combination of factors that may not be accurately captured in general trends, giving rise to a chaotic nature in the atmosphere and non-linear interactions. In addition, different regions may experience unique environmental conditions, such as local topography or oceanic currents, resulting in variations in atmospheric dynamics that influence the behavior of storms. Hence, our study aims to bridge this gap by zooming in on the particular features of extreme storms in different regions. For this reason, we employ an approach within the field of Extreme Event Attribution (EEA) (Trenberth et al. 2015; Jézéquel et al. 2018), specifically designed to address these questions. This field allows us to delve into the domain of weather science to understand the specific meteorological conditions contributing to the event while simultaneously evaluating the role of climate change in shaping its occurrence and intensity (Shepherd 2016). We use a recent EEA approach that involves finding similar events, called *analogues*, in two different time periods and comparing their key variables (Faranda et al. 2022). Some studies have adapted this methodology to be more targeted for extratropical storms (Ginesta et al. 2022) as well as for Mediterranean storms (Faranda et al. 2023).

In our study, we further adapt this EEA approach for the analysis of explosive storms. Explosive storms are characterized by a strong deepening rate in a short time period, and can produce widespread damage when they make landfall (Liberato et al. 2013; Fink et al. 2009). These storms were identified by Sanders and Gyakum (1980) as storms with a "Normalized central Deepening Rate" (NDR_c) greater than 1:

$$NDR_c = \frac{DR_{24h}}{24h} \frac{\sin(60^\circ)}{\sin(\varphi)}, \tag{1}$$

where DR_{24h} is the pressure difference over 24 hours measured at the storm center and φ is the latitude at its second time step. This definition has been challenged, especially for the Southern Hemisphere (Lim and Simmonds 2002; Allen et al. 2010), due to the fact that it may capture storms moving rapidly towards an area of climatologically lower pressure rather than storms deepening rapidly (Sinclair 1995). However, we use the historical definition by Sanders and Gyakum (1980), as our aim is to compare storms based on their similar development and pressure change rather than to assess the sensitivity of the explosive criterion.

Explosive storms, also known as "weather bombs", are mainly formed in regions of enhanced baroclinicity (Roebber 1984). In the North Atlantic, they primarily form during the boreal winter in the western part of the basin, where there is a strong horizontal temperature gradient linked to the Gulf Stream and land-sea contrast, large moisture availability and strong vertical wind shear (Reale et al. 2019; Brayshaw et al. 2009).

We focus on three explosive storms that hit different parts of Europe: Alex in October 2020, Eunice in January 2022, and Xynthia in February 2010. Unlike many EEA studies that compare the present climate with a pre-industrial climate (factual and counterfactual periods), our method uses present and future climate projections with the Community Earth System Model version 1 (CESM1). Our study aims to:

1. Evaluate how well CESM1 simulates storms with development stages similar to the three targeted storms.

2. Analyze changes in the frequency of these storms and their deepening rates in a future climate scenario, considering the scenario with the highest greenhouse gases emissions, that is, the Representative Concentration Pathway 8.5 (RCP8.5).

3. Examine changes in hazards of these events, quantified by measuring precipitation and wind speed.

4. Characterize the underlying dynamics contributing to these observed changes.

In the subsequent sections, we present the characteristics of the storms (Section 2), describe the data and methods used (Section 3), evaluate the model performance in simulating explosive storms (Section 4), analyze changes in frequency and intensity of storms (Section 5), and assess changes in climate drivers and underlying dynamics (Section 6). The conclusions of our study are presented in section 7.

2. Storm characteristics

In this section we contextualize the three storms and provide an overview of the associated impacts and meteorological drivers.

a. Storm Alex

Storm Alex occurred in early October 2020 and produced a devastating flood in the Alps region in 24 hours. Alex caused record-breaking precipitation and hurricane-force winds in France and Italy, resulting in at least 15 fatalities and over 2.5 billion euros in economic losses (WMO 2020; European State of the Climate 2020; Météo France 2020; Aon 2020). Notable events included 630 mm of rain in Sambughetto and winds reaching 186 km/h in Belle-Île - Le Talut (European State of the Climate 2020; Météo France 2020). The storm developed as a secondary cyclogenesis, that is, as a frontal-wave instability along of a synoptic front of a pre-existing storm. It deepen rapidly, enhanced by high upper level potential vorticity. The pressure dropped more than 30 hPa in the first 24 hPa. It made landfall early 2 October with a minimum pressure of around 970 hPa. On its southern flank, the strong pressure gradient favoured high quantities of water vapour transport, and an atmospheric river was formed from the subtropical western North Atlantic to the vicinity of the storm core (Davolio et al. 2022). In an EEA study based on reanalysis data (Ginesta et al. 2022), the persistence of the storm, as well as the accumulated daily precipitation, increased in the present climate when compared to the recent past climate.

b. Storm Eunice

Eunice was the second and strongest storm of a cluster of winter storms (Met Office 2022) that lasted between the 16th – 20th of February 2022 and mainly affected western Europe. The storm, also known as Storm Zeynep or Storm Nora in Germany and Denmark, respectively, caused

widespread damage, 17 fatalities, and insured losses estimated at 2.5–3.5 billion euros (NL Times 2022; Anadolu Agency 2022; Deutsche Welle 2022; BBC 2022; RTL Info 2022; The Irish Times 2022; RMS 2022). Eunice formed from secondary cyclogenesis on February 17 in the North Atlantic. It experienced explosive cyclogenesis with a central pressure drop of 30 hPa in 18 hours. On February 18 at around 6 am Eunice made landfall in Ireland and then crossed the UK in 12 hours. A wind gust of 196 km/h was recorded in The Needles, Isle of Wight, the strongest ever recorded in England. On February 18 at around 6 pm the storm was located over the North Sea reaching a sea level pressure in its core below 970 hPa, the minimum of its lifetime. In the hours that followed, the storm swept across Western Europe with force, hitting in particular Germany, the Netherlands, and Belgium.

c. Storm Xynthia

In winter 2009/2010, the general atmospheric circulation over Europe was characterized by an extreme and record-persistent negative phase of the North-Atlantic Oscillation (NAO) (Cattiaux et al. 2010). This led to a low latitudinal position of the jet stream, several severe cold spells, cold weather conditions and destructive storms. Xynthia, the strongest and most damaging storm to hit Europe in that winter, occurred in late February/early March 2010, and raised interest in the scientific community due to its uncommon meteorological characteristics (e.g. Liberato et al. 2013) and impacts (e.g. Chadenas et al. 2014; Vinet et al. 2012). It followed an unusual SW-NE path, causing significant impacts in several western European countries, including more than 60 fatalities and insured losses of 1.5–3 billion euros (García-Pereda (NWC SAF/AEMET) 2010; Kolen et al. 2013; Worlwide 2010; Chauveau et al. 2011). Unlike most extratropical storms that intensify rapidly when they cross the polar jet stream (Uccellini 1990), Xynthia's intensification was primarily driven by the advection of low-level warm, humid air and associated with high values of equivalent potential temperature (θ_e) (Fink et al. 2012). The storm underwent explosive cyclogenesis between the 26th and the 27th while rapidly approaching to the Iberian Peninsula. On the 27th at 18:00 UTC it reached its minimum sea level pressure below 970 hPa west of the Bay of Biscay. It then swept across western France, resulting in a powerful storm surge that locally exceeded 1.5 m and that produced most of the damages in France (Bertin et al. 2012).

Xynthia continued its path northeastwards hitting specially Belgium, the Netherlands, Germany and Denmark.

3. Datasets and methods

a. Datasets

To address the above objectives, we use the Community Earth System Model version 1 (CESM1; Hurrell et al. (2013)), which is a global coupled climate model with a horizontal resolution of about 1 degree. The radiative forcing applied in all simulations is the historical forcing until 2005 and the Representative Concentration Pathway 8.5 (RCP8.5) forcing from the CMIP5 project (Meinshausen et al. 2011) from 2005 onwards. We use a multimember initial condition ensemble CESM-LE (CESM-LE; Kay et al. (2015)), consisting of a 35-member ensemble of simulations from 1 January 1920 to 2100. To increase the number of members, two additional ensembles of 35 members each are performed. In both ensembles, 35 members are rerun from perturbations of $O(10^{-13})$ on the initial atmospheric temperature field of the first member of the CESM-LE, starting at 1980 and at 2081 (Röthlisberger et al. 2020). After a few years, due to the chaotic nature of the climate system, the members are in distinct states of their internal variability, and thus they are considered to be independent (Fischer et al. 2013). Hence, the experimental set-up of this study consists of 1050 years of a *present* climate, from 1991 to 2000, and 1050 years of a *future* climate, from 2091 to 2100. The radiative forcing is assumed to be relatively constant in a 10-year period. Kay et al. (2015) showed that the spread of the CESM-LE due to internal variability is comparable to CMIP5. In contrast to many CMIP5 models, CESM does not depict a too zonally oriented North Atlantic storm track (Dolores-Tesillos et al. 2022). According to Dolores-Tesillos et al. (2022), the model is able to reproduce fairly well storm frequencies and lifetimes, and most of the biases are associated to weak or short living storms. They found an underestimation of the number of storms over the ocean, of around -0.8 storms per month. At smaller scales, the model is able to represent the properties and structure of extratropical storms and their associated warm conveyor belts (Joos et al. 2023; Binder et al. 2023). The deepening rates of the weak and medium-strong storms in the NH in winter are also well captured by the model but there is an underestimation of the explosive ones (Binder et al. 2023).

In this study we also use ERA5 reanalysis data (Hersbach et al. 2020), covering the period from 1950 to 2020, as a validation of the CESM model performance. The ERA5 dataset has a horizontal resolution of 31 km.

We use 6-hourly sea level pressure (SLP) to find the analogues, and we assess the meteorological hazards using 6-hourly precipitation rate (PR), and wind speed at 10m. We define a wind severity ratio (WSR_{90}) as the ratio between the maximum wind speed within a 24-hour period centered on the minimum sea level pressure stage of the storms, divided by the 90th percentile of wind speed for the entire period ($WSR_{90} = v_t/v_{90}$). The 90th percentile for ERA5 has been computed using the entire period, while for CESM, it has been computed based on the present period.

To better assess the drivers of the changes in SLP, PR, and WSR_{90} between CESM present and future periods we further analyze the following 6-hourly variables: equivalent potential temperature (θ_e) at 850hPa, horizontal gradient of θ_e ($\nabla\theta_e$) at 850hPa, distribution of the upper-tropospheric jet stream, and the low-level Eady Growth Rate (EGR) between 850hPa and 500hPa. The distribution of the upper-tropospheric jet stream is based on the methodology outlined in Koch et al. (2006), where jet occurrence is identified by averaging wind speeds between 400 hPa and 100 hPa (to account for height variations) and exceeding a threshold of 30 m/s. EGR is computed as:

$$EGR = 0.31\frac{f}{N}\sqrt{\frac{\delta(u,v)}{\delta z}} \tag{2}$$

where $f = 2\Omega\sin\phi$ is the Coriolis parameter, $N = \sqrt{\frac{9.81}{\theta}\frac{\delta\theta}{\delta z}}$ is the Brunt-Väisälä frequency, and $\sqrt{\frac{\delta(u,v)}{\delta z}}$ is the vertical wind share. Ω is the angular velocity of the Earth ($7.29\times10^{-5} rad/s$), ϕ latitude, u and v zonal and meridional wind speeds, θ potential temperature, and z geopotential height.

b. Methods

We use the method of analogues (Yiou 2014), which has already been applied to the study of extratropical storms (Ginesta et al. 2022; Faranda et al. 2023), to find similar storms to Alex, Eunice, and Xynthia. In the context of this study, an analogue is defined as a storm with a similar development stage or a comparable track during its evolution, which is explosive if the NDR_c is higher than 1 according to equation (1). The full tracks of storms Alex, Eunice, and Xynthia are

shown in figure A2 in the Appendix. We define the development stage of the storms as the 24h period before reaching their mature stage (figure A2 of the Appendix from points 0 to 1). First, we identify and track all storms in each dataset (ERA5, CESM present, CESM future). We use a Lagrangian approach where storms centers are defined and tracked as local minima in the sea-level pressure field (Wernli and Schwierz 2006). We then select the storms that have the most similar development stages to the targeted storms based on our definition of analogue. For that, we apply a two-step process:

- We first select all storms in the database that have a minimum sea level pressure lower than 1000 hPa and located within a circle of radius 300 km of the targeted storm center in its minimum sea level pressure point. This filter ensures that only storms in their mature stage are considered and that they have reached their minimum sea level pressure in the vicinity of the targeted storm's center region. We refer to these storms as *mature stage* storms, and the time when they reach their minimum sea level pressure is defined as *time 0*.

- We select the last five grid points of the development stage of the mature stage storms. As we use 6-hourly data, this corresponds to the tracks 24 hours before the time 0 dates. For each mature stage storm, we compute the averaged Euclidean distance between the track of the storm and the track of the targeted storm. We select the 20% mature stage storms with the lowest Euclidean distance from the targeted storm. This corresponds to the 20% most similar development stage tracks. We term these *analogues*. The decision to use 20% is a trade-off between finding tracks that resemble those of the targeted storms and having a sufficiently large sample size to draw meaningful statistical conclusions. We tested that altering the percentage to 10%, 15%, or 25% does not significantly impact our findings. We also select the analogues that undergo explosive cyclogenesis, that is, that have a NDR_c greater than 1 (Eq. (1)). We term these *explosive analogues*.

4. Representation of explosive storms in CESM present-day climate

Figure 1 shows the frequency of mature stage storms every 10 years for ERA5 (a) and CESM present climate (b), as well as the frequency every 100 years of those that are explosive (c,d). As noted by Dolores-Tesillos et al. (2022), there is an underestimation of storm numbers in the model compared to observations, particularly evident in the ocean. Furthermore, we observe an

underestimation of mature stage storms west of Newfoundland, especially the explosive ones. In the regions studied, highlighted in red, we note a slight underestimation of both mature stage storms and explosive ones, especially in the North Sea. However, the bias is considerably smaller in these regions compared to the ocean. Despite the small proportion of storms assessed in this study compared to the overall North Atlantic basin, these three regions are highly susceptible to widespread damage when such storms make landfall, and the selected storms and their analogues represent a significant portion of weather bombs impacting these areas.

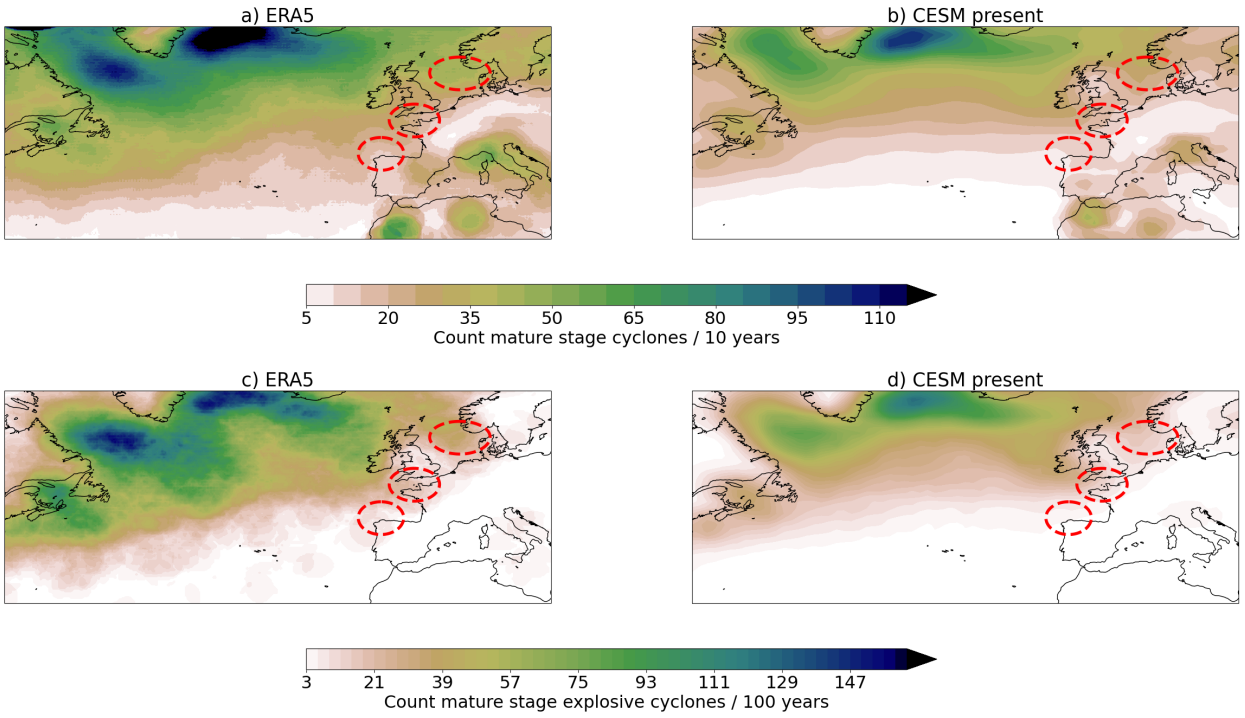

FIG. 1. Frequency of mature stage cyclones within 300 km for each grid point every 10 years for (a) ERA5 and (b) CESM present. (c,d) Frequency of those that are explosive, every 100 years. Red circles indicate the 300-km radius area used to identify analogues of the three storms.

Figure 2a shows the NDR_c of both ERA5 and CESM, similar as Binder et al. (2023) did for the Northern and Southern Hemispheres but focused on the North Atlantic. Figure 2b shows the differences between CESM present and ERA5. Consistent with their findings, we also identify a slight underestimation of the NDR_c of the most explosive storms in the basin, of up to around -0.2 in the most extreme cases. However, there is strong agreement across almost all percentiles.

This comparative analysis, together with assessments by Dolores-Tesillos et al. (2022) and Binder et al. (2023), gives confidence in the model capability to simulate explosive storms making landfall on the western coast of Europe. Further exploration of the model ability to simulate analogues of the storms will be conducted in the subsequent section.

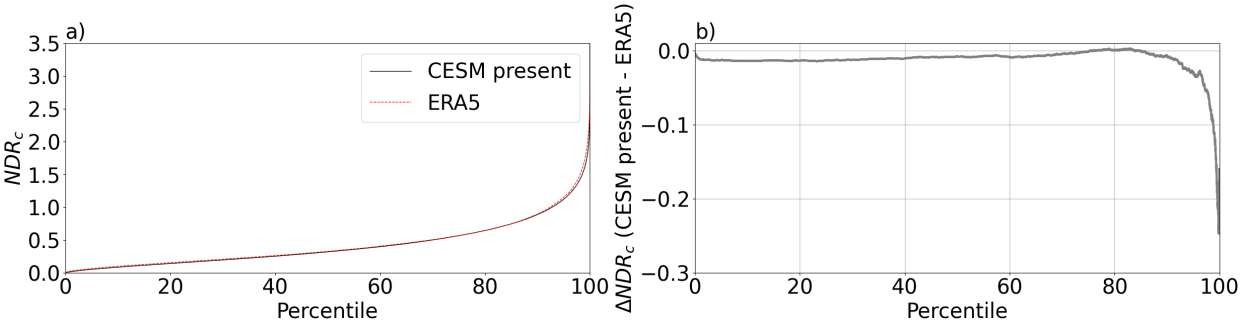

FIG. 2. a) Percentile curve of the Normalized central Deepening Rate (NDR_c) of storms in the North Atlantic for ERA5 and CESM present. b) Differences in the NDR_c between CESM present and ERA5.

5. Changes in frequency and intensity

In this section, we first validate the CESM model performance in simulating analogue storms of Alex, Eunice, and Xynthia, using ERA5 reanalysis data. Then, we assess future changes in frequency of occurrence and intensity, measured by the NDR_c, by comparing CESM present and future climates.

a. Storm Alex

Figure 3 shows the tracks during the development stage of the analogues and explosive analogues of Alex for each dataset. The legends also display the number of analogues and explosive analogues. In the ERA5 70-year period, 63 analogues have been identified, that is, around 9 analogues every 10 years. In contrast, fewer analogues are detected in the CESM present climate, with a frequency of almost 3 analogues every 10 years. This could be due to an underestimation of storm frequencies over the ocean (Dolores-Tesillos et al. 2022). In the ERA5 dataset, 10 of the 63 analogues are explosive, corresponding to a relative frequency of around 16% of the analogues. Three of these explosive analogues are known storms that made landfall in France (Table A1). The fraction of analogues that are explosive in the CESM present period is slightly lower than that of ERA5 (34

explosive analogues out of 299 analogues, that is, around 11%). The NDR_c, used here as a measure of the intensity, of the analogues and explosive analogues in CESM present is comparable to that of ERA5. We further measure the similarity of the analogues to the storm by computing the mean Euclidean distance between the 24-hour development stage tracks of the analogues and storm Alex. We term this *analogues quality* (Figs. 4a,c). The analogues quality distributions of CESM present show comparable values with ERA5, as no analogue was more than 500 km apart and most of them differed by around 380 km. These distributions indicate the model ability to simulate storms with development stage similar to Alex's. Figures 4b,d show the number of analogues per season. Most of the analogues occur in autumn season in both ERA5 and CESM present. However, in ERA5 the second most preferred season is spring, while in CESM present is winter. Few analogues are also detected in summer in both, ERA5 and CESM present.

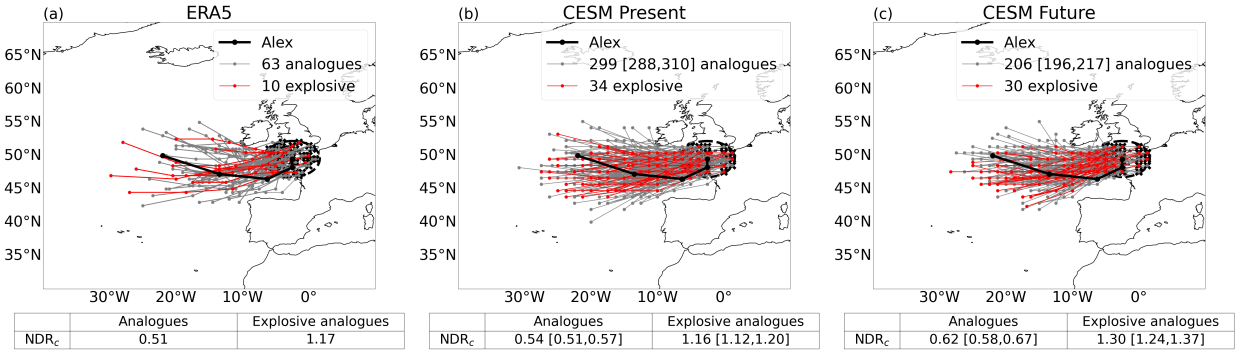

	Analogues	Explosive analogues
NDR_c	0.51	1.17

	Analogues	Explosive analogues
NDR_c	0.54 [0.51,0.57]	1.16 [1.12,1.20]

	Analogues	Explosive analogues
NDR_c	0.62 [0.58,0.67]	1.30 [1.24,1.37]

FIG. 3. 24-hour track of the development stage of storm **Alex** (thick black line) and its analogues (thin grey lines), for ERA5 (a), CESM present (b), and CESM future (c). Explosive analogues' tracks are highlighted in red. The dashed-line circle indicates the 300-km area used to identify mature stage storms. The figure legend shows the number of analogues and explosive analogues. The tables beneath the figures depict the Normalized Deepening Rate (NDR_c) values, calculated using equation 1, for both analogues and explosive analogues. 95 % confidence intervals for CESM present and CESM future, determined using a bootstrap test in which ensemble members were resampled, are indicated in brackets. The NDR_c values are also shown in figure A1 as a boxplot distribution.

There is a statistically significant decrease in the number of analogues in the future climate with respect to the present from 299 to 206 (Fig. 3). This decrease is mainly seen in autumn and summer, but there is also a slight decrease in winter and spring (Fig. 4b). There is little change in the number

of explosive analogues (34 to 30) (Fig. 3), with a decrease in frequency mainly in autumn (Fig. 4d). The relative frequency of explosive storms increases from present to future periods from 11% to 15%. However, this increase is comparable to the model bias, suggesting that while the model can detect a significant climate change signal, uncertainties regarding its magnitude may arise due to model biases. There is an increase in NDR_c of both analogues and explosive analogues in the future climate with respect to the present, which is considered statistically significant because the confidence intervals do not overlap. This suggests that the analogues and explosive analogues in the future climate will be associated with more intense deepening rates. In addition, the analogues travel larger distances during their development stage in the future period (not shown). Regarding the quality of the analogues, there is a statistically significant increase in the future period with respect to the present (Fig. 4a). This indicates that analogues in future conditions resemble better Alex's development stage than in the present climate. In summary, anthropogenic radiative forcing is reducing the number of analogues of Alex, specially in autumn, but increasing their similarity to the storm as well as the deepening rates.

b. Storm Eunice

In ERA5 we found 126 analogues, that is, around 18 every 10 years (Fig. 5). However, CESM again underestimates the number of analogues, detecting 6–7 every 10 years in the present climate (696). 23 out of 126 analogues are explosive in the ERA5 dataset, of which 8 are documented storms that had an impact in Europe (Table A1). This corresponds to a relative frequency of explosive storms of 18.3%. The relative frequency of analogues that undergo explosive cyclogenesis in the CESM present is half of that of ERA5 (9.6%). In addition, the NDR_c of the analogues and explosive analogues is slightly lower in the model than in ERA5 for both present analogues and explosive analogues. Regarding the quality of the analogues (Fig. 6a), the analogues detected by the model have lower mean Euclidean distances than those detected by ERA5. This indicates that the model is good at reproducing storms that resemble Eunice's development stage. In the ERA5 dataset, most of the analogues are found in autumn, while winter and summer have a similar frequency (Fig. 6b). In the CESM present, the number of analogues in winter is slightly higher than than in autumn.

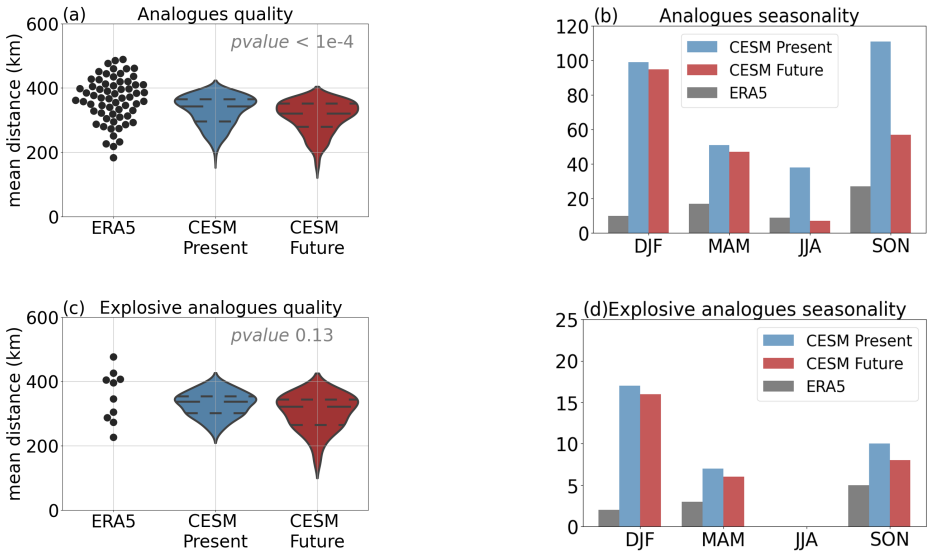

FIG. 4. (a,c) Mean Euclidean distances between the 24–hour track of the development stage of storm **Alex** and its **analogues** and explosive analogues for ERA5 (black dots), CESM present (blue probability distribution), and CESM future (red probability distribution). Dashed lines in violin plots show the quartiles 25%, 50%, and 75%. A Kolmogorov-Smirnov test was used to determine the statistically significant difference between CESM present and future distributions, with the resulting p-value indicated in the figure. (b,d) Number of analogues per season: SON (September, October, November), DJF (December, January, February), JJA (June, July, August), and MAM (March, April, May).

Despite no significant changes in the number of analogues in the CESM future climate with respect to the present climate (Fig. 5b,c), there is a decrease in frequency in autumn, summer and spring, and an increase in winter (Fig. 6b). In the case of explosive storms, there is a significant increase in the number of explosive analogues (67 to 95), corresponding to an increase in the relative frequency of explosive cyclogenesis in a future climate. This increase is mainly seen in winter (Fig. 6d), and a decrease again in autumn. The NDR_c of the analogues increases in a future climate (Fig. 5b,c), but there are no significant changes in NDR_c of the explosive analogues. In the future climate, the analogues and explosive analogues quality is better than in the present, as evidenced by the statistically significant differences in probability distributions (Fig. 6a,c). As also seen in Figure 5, the spatial spread in the development stage tracks of the analogues is lower in the future climate, which means that future analogues represent Eunice's tracks better than those in the present. In summary, there is a significant increase in the frequency of explosive cyclogenesis

in the future climate in winter. Additionally, the quality of analogues and explosive analogues improves significantly in the future. These changes collectively suggest an increased likelihood of Eunice-type storms in the future climate in winter.

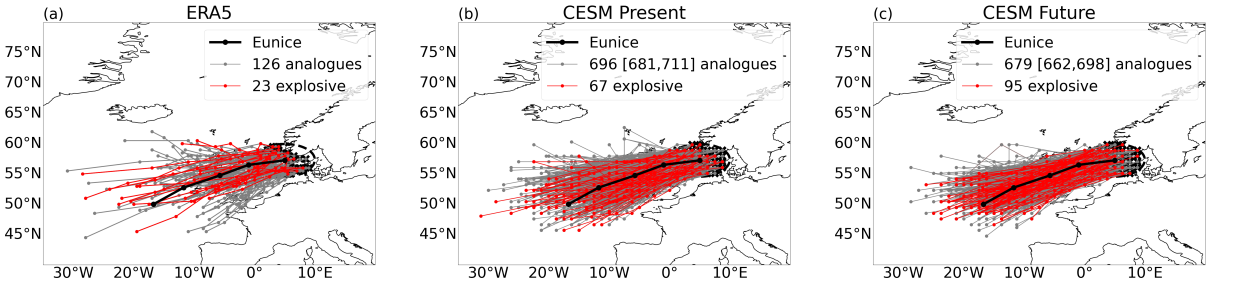

	Analogues	Explosive analogues
NDR_c	0.55	1.26

	Analogues	Explosive analogues
NDR_c	0.53 [0.51,0.55]	1.21 [1.18,1.24]

	Analogues	Explosive analogues
NDR_c	0.61 [0.58,0.62]	1.23 [1.20,1.27]

FIG. 5. Same as figure 3 but for storm **Eunice**.

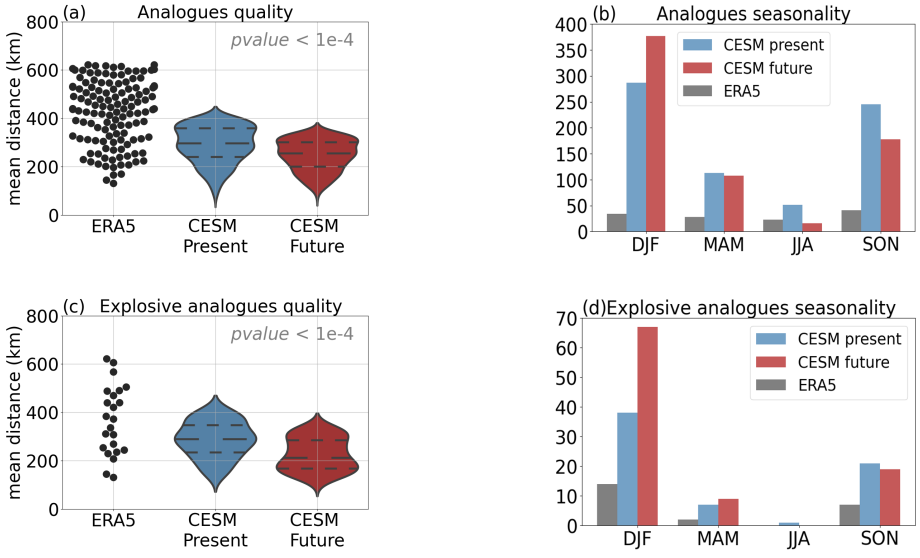

FIG. 6. Same as figure 4 but for storm **Eunice**.

c. Storm Xynthia

About 5 analogues every 10 years are detected in ERA5 and almost 1 every 10 years in the CESM present dataset (Fig. 7). This suggests that the CESM model underestimates the number of analogues that reach Galicia in their mature stage, linked to an underestimation of the storm frequency in that region shown by Dolores-Tesillos et al. (2022). In terms of explosive occurrence, 3 out of 38 analogues underwent explosive cyclogenesis in ERA5 period, that is, around 8% of the

analogues. One of these is Miguel, a storm that affected western Europe in 2019 (Table A1). In the CESM present, the fraction of analogues that undergo explosive cyclogenesis is higher than in ERA5 (14 out of 101, that is, around 14%). In addition, the NDR_c of the analogues of the CESM present is higher than in ERA5. Despite the possible model biases, figures 8a,c show that the analogues and explosive analogues quality of the CESM dataset is comparable to that of the ERA5 period. In ERA5 the analogues occur more often in autumn, while in the CESM present dataset it is in spring (Fig. 8b). In terms of the relative change between present and future climates, there is a significant decrease in the number of analogues in the future climate (101 to 68) (Fig. 7b,c). This decrease occur specially in spring, but also in autumn and summer (Fig. 8b). The number of explosive storms decreased slightly (from 14 to 11), with a decrease in spring and autumn but an increase in winter (Fig. 8d). Hence, there is an increase in the relative frequency of explosive storms, from around 14% to 16%. The NDR of the explosive analogues increases significantly under future climate conditions. However, due to the overlap in the confidence intervals, it is not possible to conclude that this increase is statistically significant, likely due to the insufficient sample size. No statistically significant changes are found in the analogues quality distributions between the two periods (Fig. 8a,c).

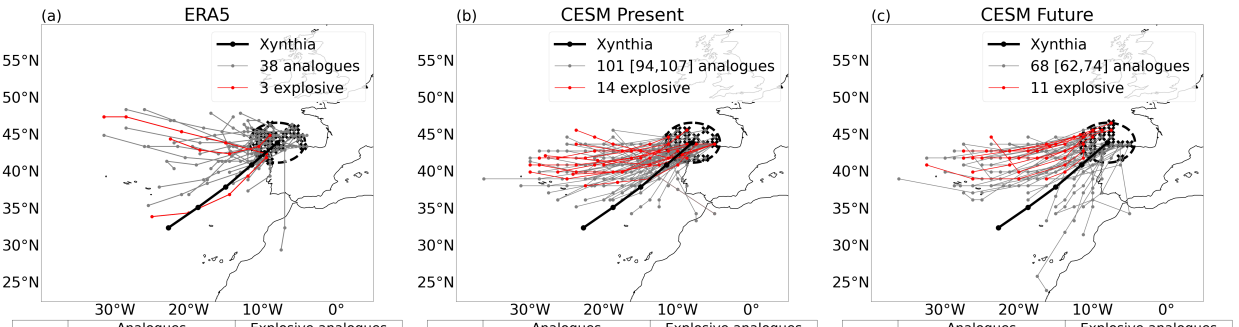

	Analogues	Explosive analogues
NDR_c	0.47	1.25

	Analogues	Explosive analogues
NDR_c	0.50 [0.43,0.56]	1.27 [1.17,1.36]

	Analogues	Explosive analogues
NDR_c	0.60 [0.51,0.69]	1.48 [1.30,1.59]

FIG. 7. Same as figure 3 but for storm **Xynthia**.

6. Meteorological hazards and Dynamics

In this section, we analyze changes in the fields of precipitation and wind severity ratio. To gain deeper insights into the evolving patterns of explosive analogues, we also assess the atmospheric dynamics contributing to these changes.

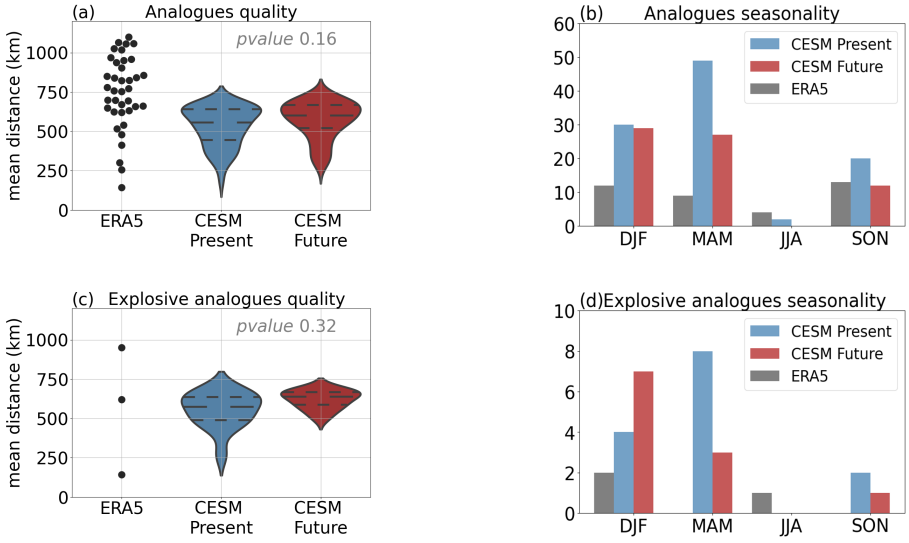

FIG. 8. Same as figure 4 but for storm **Xynthia**.

a. Storm Alex

Figures 9a,b,c show the sea–level pressure (SLP), precipitation rate (PR), and wind severity ratio (WSR_{90}) fields of storm Alex using ERA5 data at its time 0 date. The minimum SLP is around 970 hPa, and the storm center is squeezed over the English channel. Regarding PR, precipitation is primarily located along the storm's frontal structure, as well as over the Southeastern France coast and windward of the Alps. High WSR_{90} is predominantly observed in the southwestern section of the storm. The CESM present composites of analogues and explosive analogues for SLP, PR and WSR_{90} are shown in black contours in figures 9d–i as well as in figure A3 in the Appendix. As expected, the pressure gradient in the explosive analogues composites is higher than that in the analogues (higher and closer number of black contours in Fig. 9g,d, respectively), resulting in lower SLP values in the storm core. In addition, explosive analogues are associated to higher PR and WSR_{90} (black contours in Fig. 9h,i, respectively) than those of the analogues (Fig. 9e,f, respectively). SLP composites of both CESM present analogues and explosive analogues (Fig. 9d,g) depict a cyclonic structure with the center over the English channel, consistent with Alex. With respect to the PR pattern, this is predominantly located within the storm core and its southern region (Fig. 9e,h). Due to the lack of precise alignment of storm fronts among the analogues, the PR pattern does not display a clearly defined frontal area. High values of WSR_{90} are located in the center and southern flank of the storm (Fig. 9f,i).

Shading in figures (Fig. 9d–f) show differences CESM future – minus – present of the analogues composites for SLP, PR, and WSR_{90}, respectively. The analogues in the future period show positive anomalies of SLP northward of the Azores anticyclone as well as in the eastern Mediterranean (Fig. 9d). This contributes to increase the amplitude of the Rossby waves. In addition, there are SLP negative anomalies in the core of the analogues. This means that the analogues in the future period are associated to lower core pressures and to an increased pressure gradient. This, in turn, might be linked to increase WSR_{90} in the future period in the southern flank and over land (Fig. 9f). Despite a decrease in the center and northern flank, there is an overall increase in WSR_{90} associated with the analogues. In addition, PR increases, specially to the east of the storm core, in the future period (Fig. 9e). The SLP differences of the explosive analogues depict a similar structure to that of the analogues (Fig. 9g), with deeper storms in the future period and positive anomalies on the eastern Mediterranean and southern Scandinavia. This increase in the SLP gradient is also reflected by an increase in WSR_{90} (Fig. 9i), which is particularly high over land, especially in the UK and western France, Belgium, and the Netherlands. Figure 9h depicts an increase of PR in the northern flank analogues' core and a decrease, albeit smaller, southward.

The PR and WSR_{90} patterns of extratropical storms such as Alex and its analogues are mostly influenced by the position and intensity of weather fronts. To assess changes in the weather fronts, we evaluate the equivalent potential temperature at 850 hPa pattern (θ_e, figures 10a,b). We also compute the gradient of the θ_e field ($\nabla\theta_e$). The regions of the maximum $\nabla\theta_e$ are shown by white dashed lines in figures 10a,b, typically characterizing the presence of weather fronts. Figure 10c illustrates the future minus present differences in $\nabla\theta_e$, providing insights into the changes in front positions. In the CESM future, θ_e is overall higher than in the present, as a result of the expected increase in global temperatures and water vapour content in a changing climate (shading in Fig. 10a,b). Regarding the regions of maximum $\nabla\theta_e$ (white dashed line in Fig. 10a,b), we interpret that a cold front originates southwestern France and extends towards north of the Azores, as it is typically characterized by cold temperatures behind the warm sector. The other regions of maximum $\nabla\theta_e$ are over English Channel extending towards central western Europe, and they would be associated to the occluded and warm fronts, respectively. Regarding the future minus present differences in $\nabla\theta_e$, we see a noticeable increase and a slight southward shift along the position of the cold front (Fig. 10c). We also observe a northwestward shift in the warm front. These shifts

lead to a relocation of weather fronts of the explosive analogues in the future climate compared to the present, potentially indicating a more rapid development of storms.

We also assess the upper-tropospheric jet stream distribution (Fig. 11) at the time 0 dates. Figures 11a and b show that the jet stream is situated in the southern flank and slightly westward of the low-level cyclone. Hence, the surface low is located at the left exit region of the jet streak. This configuration is typical of storms at their maximum intensity. In the future period, there is an extension and consequent intensification of the jet downstream and southward compared to the present composites. This downstream intensification may be associated with stronger upper-level divergence, an increase in ascent airflow, and consequently, an increase in storm intensity and precipitation.

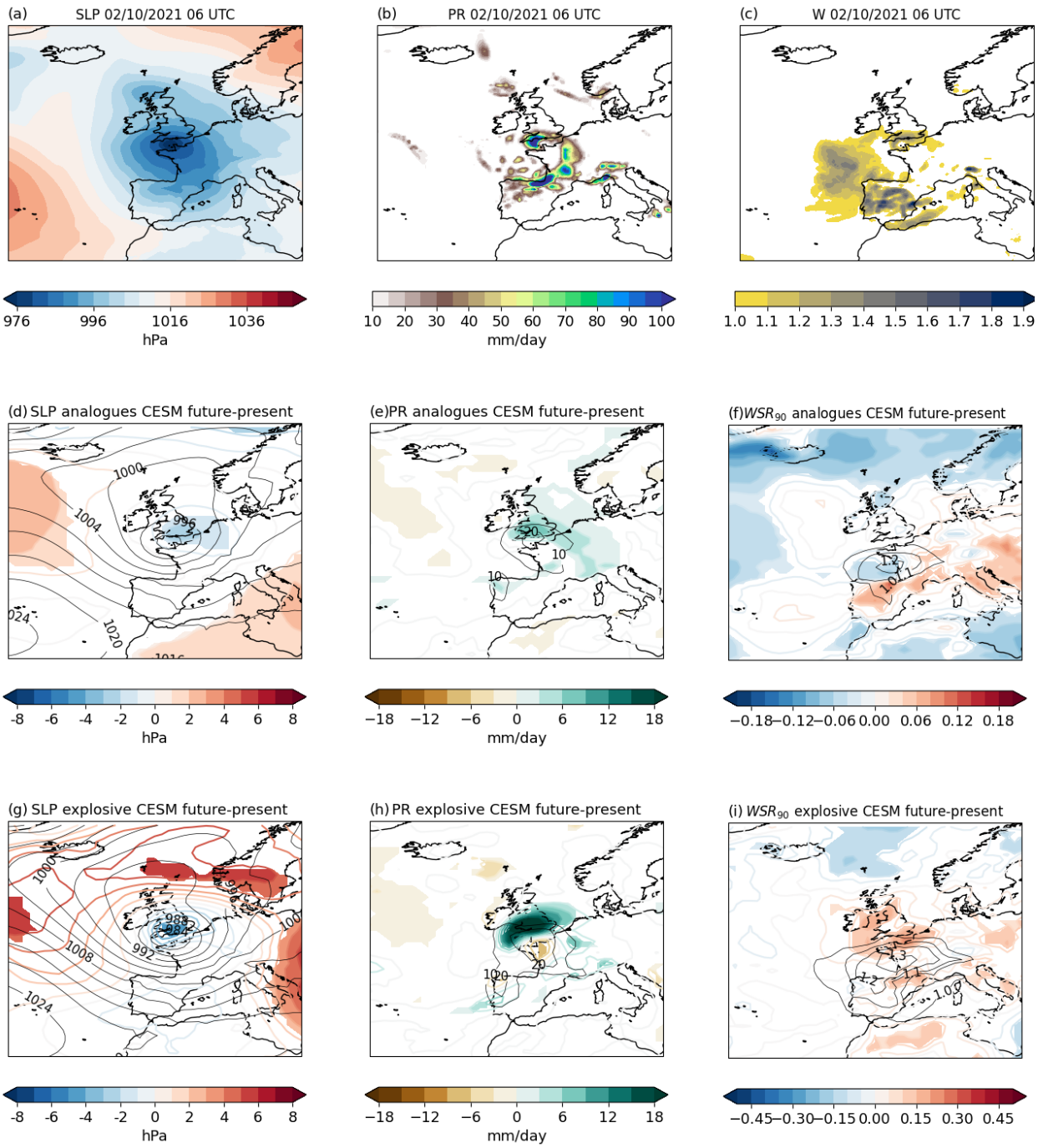

FIG. 9. (a) Sea level pressure (a), (b) precipitation rate, and (c) wind severity ratio *Alex* at time 0 using ERA5 data. (d–i) Black contours: Composites of the CESM present **analogues** and **explosive analogues** of storm **Alex** at their *time 0* dates of (d,g) sea-level pressure, at 4 hPa intervals, (e,h) hourly mean precipitation rate, from 10 mm/day and every 5 mm/day, and (f,i) hourly wind severity ratio, from 1.0 and every 0.1. Black contours are the same than shading in figure A3. Coloured contours: CESM future minus present differences of the composites of the analogues. Shading: CESM future minus present statistically significant differences, in which we bootstrapped the analogues of future and present periods. The null hypothesis of no difference is rejected if the absolute value of the difference exceeds the 95th percentile of the bootstrap distribution.

To further link changes in PR and WSR_{90} of explosive analogues with the dynamics and possible drivers, we assess the changes in eady growth rate (EGR, equation 2), convective precipitation (PRECC), and large-scale precipitation (PRECL). We observe a slight increase in EGR 24 hours prior to the mature stage of the storms, indicating an enhanced baroclinicity in future explosive analogues compared to the present (Fig. 12a). This could be linked to an increase in the NDR (Fig. 3b,c) and in the severity of storms in terms of wind speed (Fig. 9i). Furthermore, during the mature stage of the storms, we observe an overall increase in both PRECC and PRECL (Fig. 12b,c). Notably, PRECL contributes the most to the spatial changes observed in total precipitation (Fig. 9h). These changes in the PRECL pattern might be linked with the cyclonic shift of the weather fronts seen in figure 10c and changes in the stratiform precipitation produced by the warm conveyor belt.

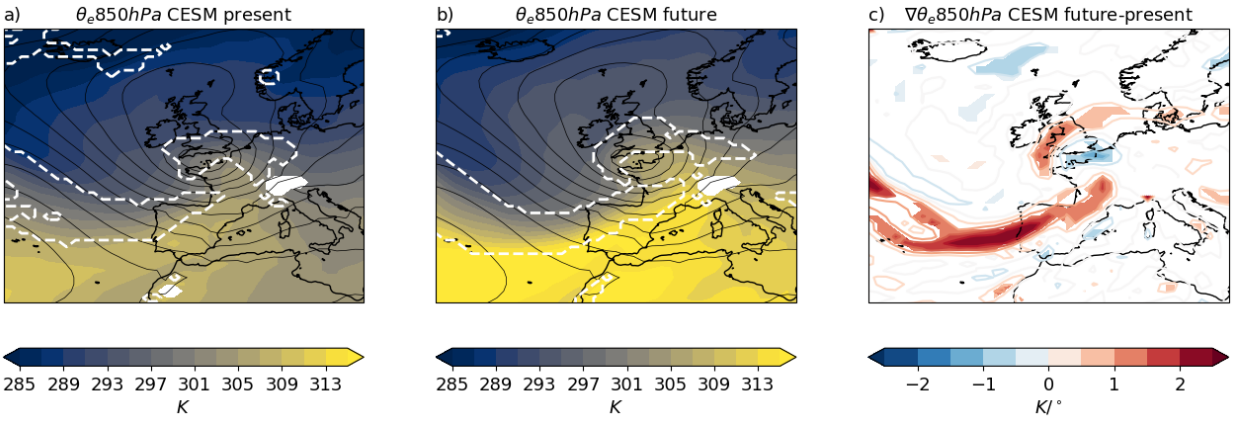

FIG. 10. (a,b) Shading: equivalent potential temperature at 850hPa for CESM (a) present and (b) future **explosive analogues** of **Alex** at their time 0 dates. White dashed lines: values exceeding the 80th percentile of the equivalent potential temperature gradient at 850 hPa. Black contours: composites of SLP at 4 hPa intervals (same as the shading in figure A3). (c) CESM future minus present differences in the composites of the horizontal gradient of equivalent potential temperature at 850 hPa.

b. Storm Eunice

Storm Eunice was situated over the North Sea during its mature stage (Fig. 13a). At that time, precipitation was relatively modest along a frontal line (Fig. 13b), while wind speeds were notably high, especially on the southern flank of the storm and over land (Fig. 13c). The composites of

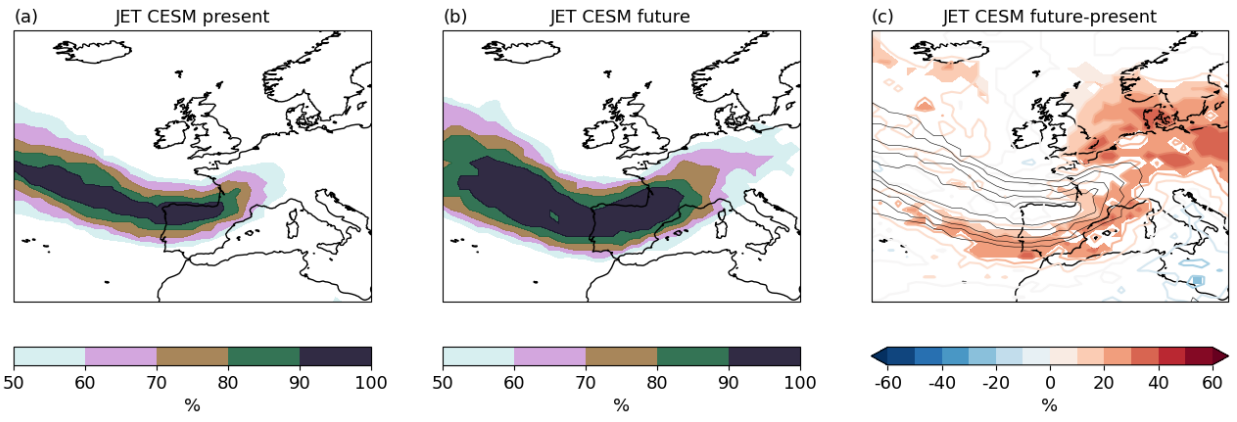

FIG. 11. Distribution of the jet events for CESM (a) present and (b) future **explosive analogues** of **Alex** at their time 0 dates. (c) Shading: CESM future minus present differences in the distribution of the jet events. Black contours: CESM present composite of the distribution of the jet events.

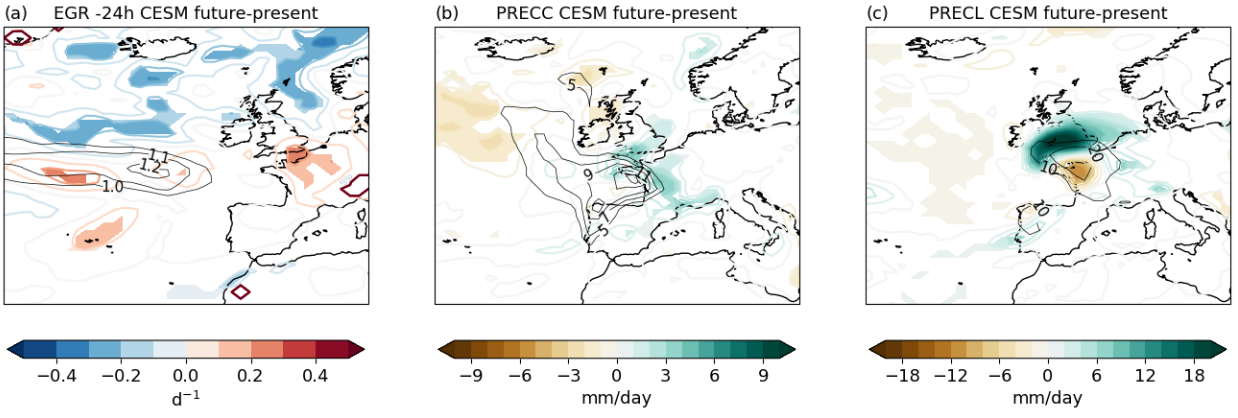

FIG. 12. Shading: CESM future minus present differences in the composites of **explosive analogues** of (a) Eady growth rate 24 hours before the time 0 dates (EGR), (b) convective precipitation (PRECC), and (c) large-scale precipitation (PRECL), respectively. Black contours: composites of CESM present of EGR, PRECC and PRECL (shadings in Figures A4).

analogues and explosive analogues exhibit similar patterns of SLP, represented by black contours in figure 13d,g, respectively, and shading in figure A5a, d. In addition, the positions of highest PR and WSR_{90} in both analogues and explosive analogues (A5e,f and A5h,i) coincide with those of storm Eunice. Explosive analogues show, as expected, lower pressure at their core, and higher PR and WSR_{90} than the analogues.

The SLP pattern of the future analogues depicts lower pressures in the cyclonic structure and higher pressures in the anticyclonic with respect to the present analogues (Fig. 13d). This is linked to deeper analogues as well as an increase in the SLP gradient in their southern flank. The PR pattern depicts an increase downstream of the analogues center and extended in western Europe (Fig. 13e), potentially linked to an increase in the uplift of moist air in the warm conveyor belt associated with lower pressure cores. In terms of WSR_{90}, there is also an increase in the southern and eastern part of the analogues over land (Fig. 13f), which corresponds to the warm sector. The differences in the patterns of explosive analogues depict a similar pattern than the analogues: lower SLP, increase in PR, and stronger WSR_{90} specially over land (Fig. 13g,h,i).

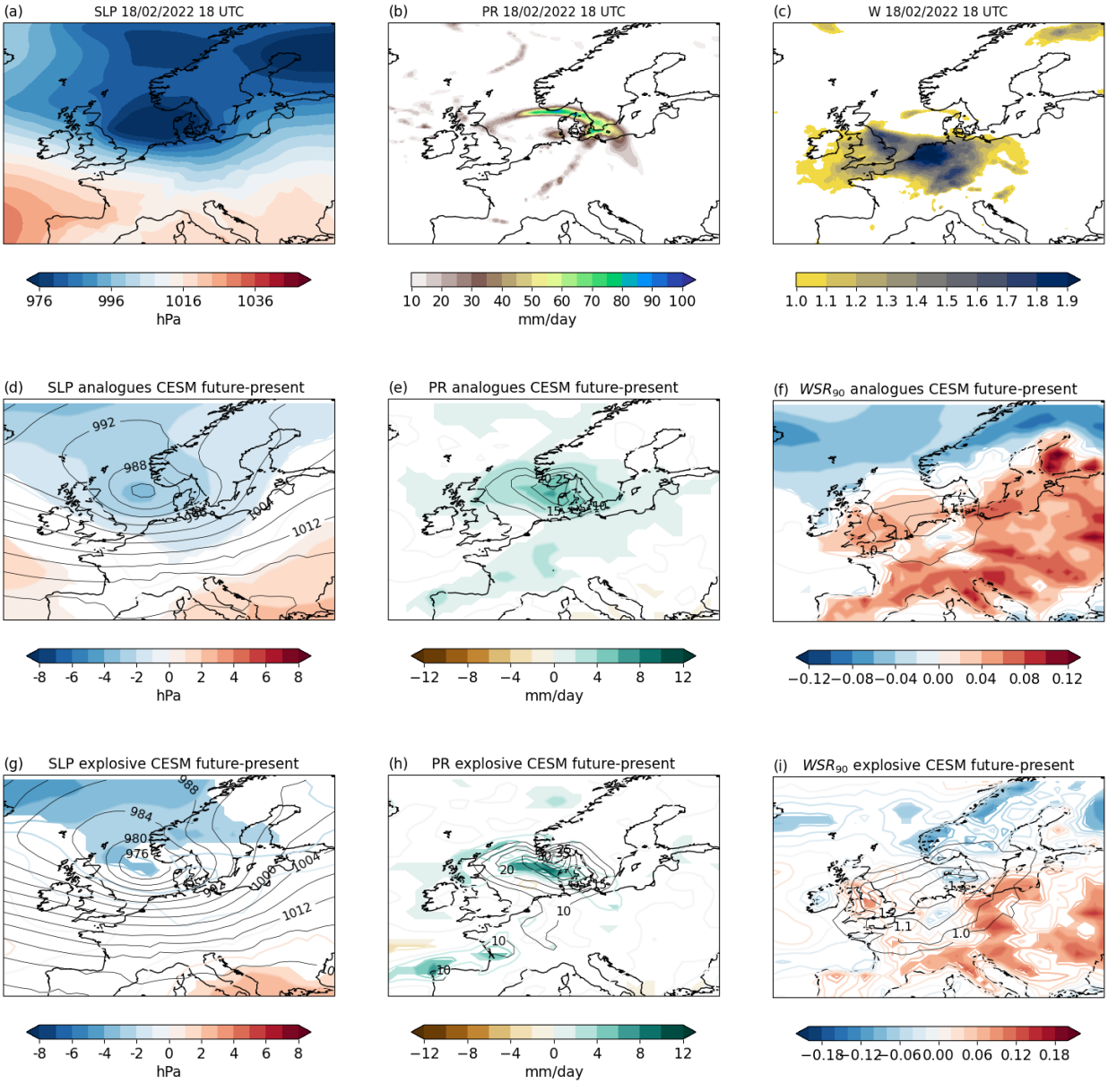

FIG. 13. Same as figure 9 but for **analogues of Eunice**.

Regarding the changes in $\nabla\theta_e$, figure 14c depicts an increase along a line starting in Germany and crossing central France and Bay of Biscay. This region corresponds to the southern flank of the cold front in the present climate, depicted in figure 14a in dashed white lines. Hence, the increase in $\nabla\theta_e$ can be interpreted as an intensification and a slight cyclonic shift of the cold front. This, in turn, might be linked to the increase in WSR_{90} (Fig. 13i) and increase in PR over the cold front area (Fig. 13h). On the contrary, a dipole pattern of $\nabla\theta_e$ over south Scandinavia suggests a deceleration of the warm front, shown in figure 14a as the tail of the comma-shape white dashed region.

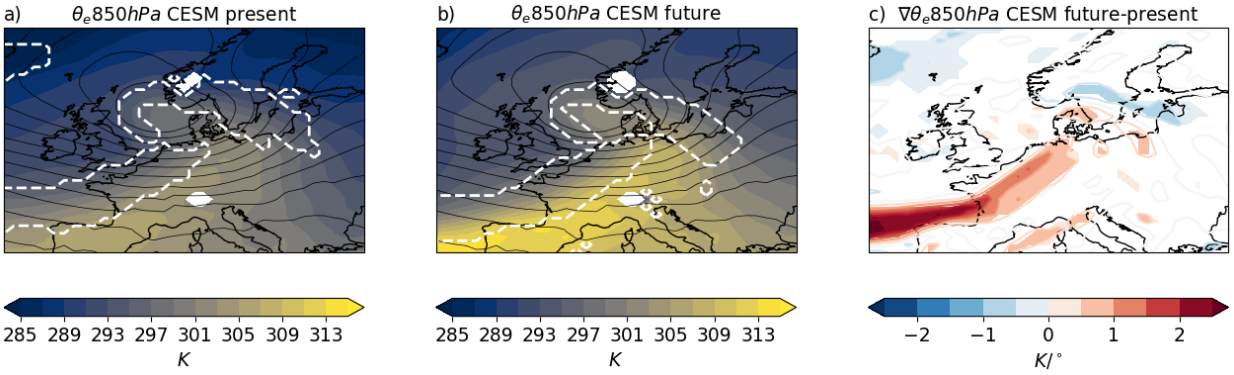

FIG. 14. Same as figure 10 but for storm **Eunice**

Figures 15a,b show that the jet stream is located southward and westward relative to the surface low. In the future period, the jet intensifies and extends further south. This suggests a localized increase in baroclinicity. Additionally, there is a slight increase in the northward flank exit region of the jet, which may be associated with an increase in upper-level divergence and ascent vertical motion.

Figure 16a shows a significant increase in the EGR 24 hours before the time 0 dates of the explosive analogues in a future period. This suggests that the changes in intensity and patterns of the explosive analogues are largely baroclinically-driven. Little changes are seen in PRECC (Fig. 16b), with an increase in the cold sector of the storm. Regarding the PRECL pattern, figure 16c shows an increase over Bay of Biscay, probably linked to the increase in intensity of the cold front, as well as an increase over Denmark, where the warm front is located.

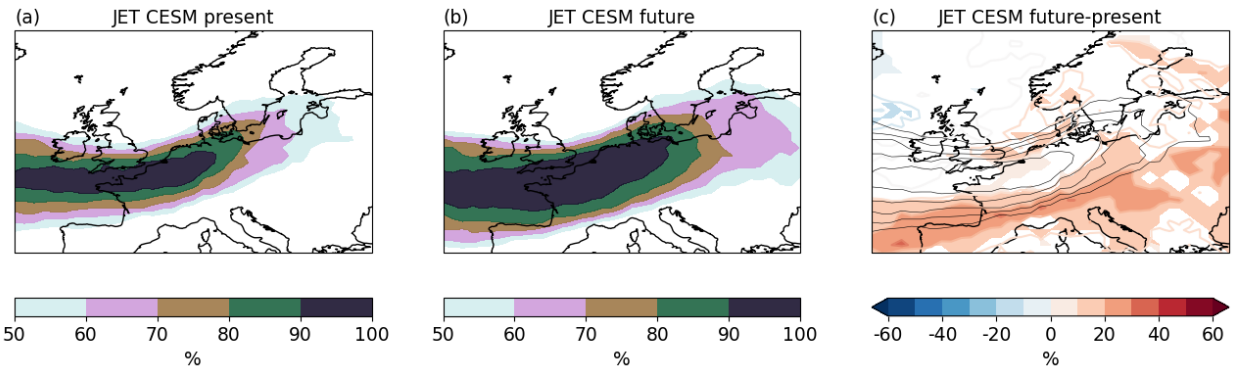

FIG. 15. Same as figure 11 but for storm **Eunice**

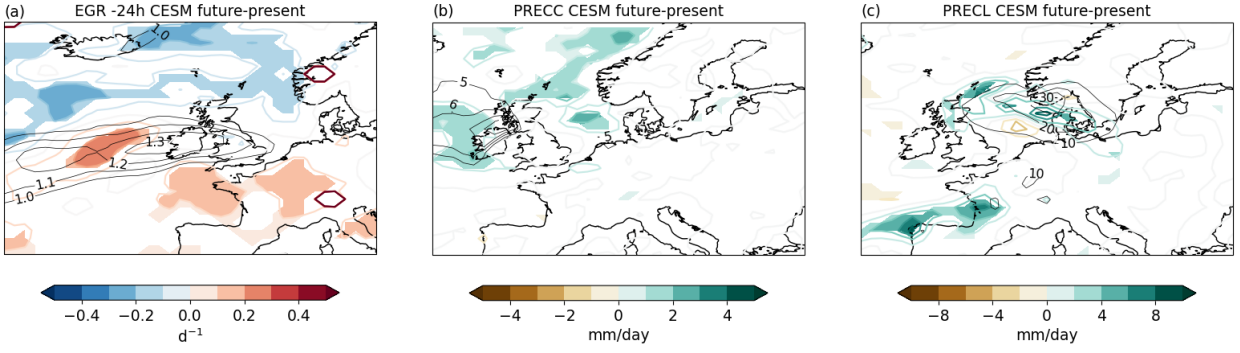

FIG. 16. Same as figure 12 but for storm **Eunice**

c. Storm Xynthia

The mature stage of storm Xynthia was situated over the Bay of Biscay (Fig. 17a). PR was primarily concentrated on the western flank of the storm (Fig. 17b), and the highest WSR_{90} was in the southern flank (Fig. 17c). In this context, both analogues and explosive analogues successfully capture the mature stage's position (Fig. 17d,g). Regarding the pattern of PR (Fig. 17e and Fig. 17f), it is slightly shifted southwards, probably due to a misalignment between the storm fronts. Similar to storms Alex and Eunice, explosive analogues demonstrate lower SLP and higher PR and WSR_{90} than the analogues.

Figure 17d depicts lower pressures in the north part of the core of the analogues. In addition, there are positive anomalies of SLP in both western and eastern of the cyclonic structure, which results in an increase in the waviness of the pressure pattern. In the case of PR and WSR_{90}, both show an increase in the analogues core and northeastern of the Iberian Peninsula (Fig. 17e,f).

Figure 17g shows that explosive analogues depict significant lower pressures in the future period, specially in their northern flank. This is linked with a significant increase in WSR_{90} (Fig. 17i). Similarly to Alex (Fig. 9h), PR depicts a significant increase in the northern flank of the explosive analogues' core, a slight decrease in the region of maximum PR in the present period, and a slight increase in their southern flank.

Figures 18a,b show a different spatial pattern of θ_e at 850hPa of present and future explosive analogues of Xynthia. In the present period, the warm sector of the storm does not overlap with the storm center. In contrast, in the future period the θ_e at 850hPa pattern has a T-bone structure, typical of the Shapiro–Keyser storms (Shapiro and Keyser 1990), and that could indicate a warm seclusion sector of the storms. In terms of changes in the gradient of θ_e, there is an overall increase of the gradient in the regions of the maximum gradient depicted by white dashed lines in 18a,b, which are the regions associated to the weather fronts. This is related to an increase in intensity of the weather fronts. A dipole with negative anomalies over the Bay of Biscay and positive anomalies northwestward suggest a cyclonic shift of the warm front position, even though the overall change is an increase in magnitude.

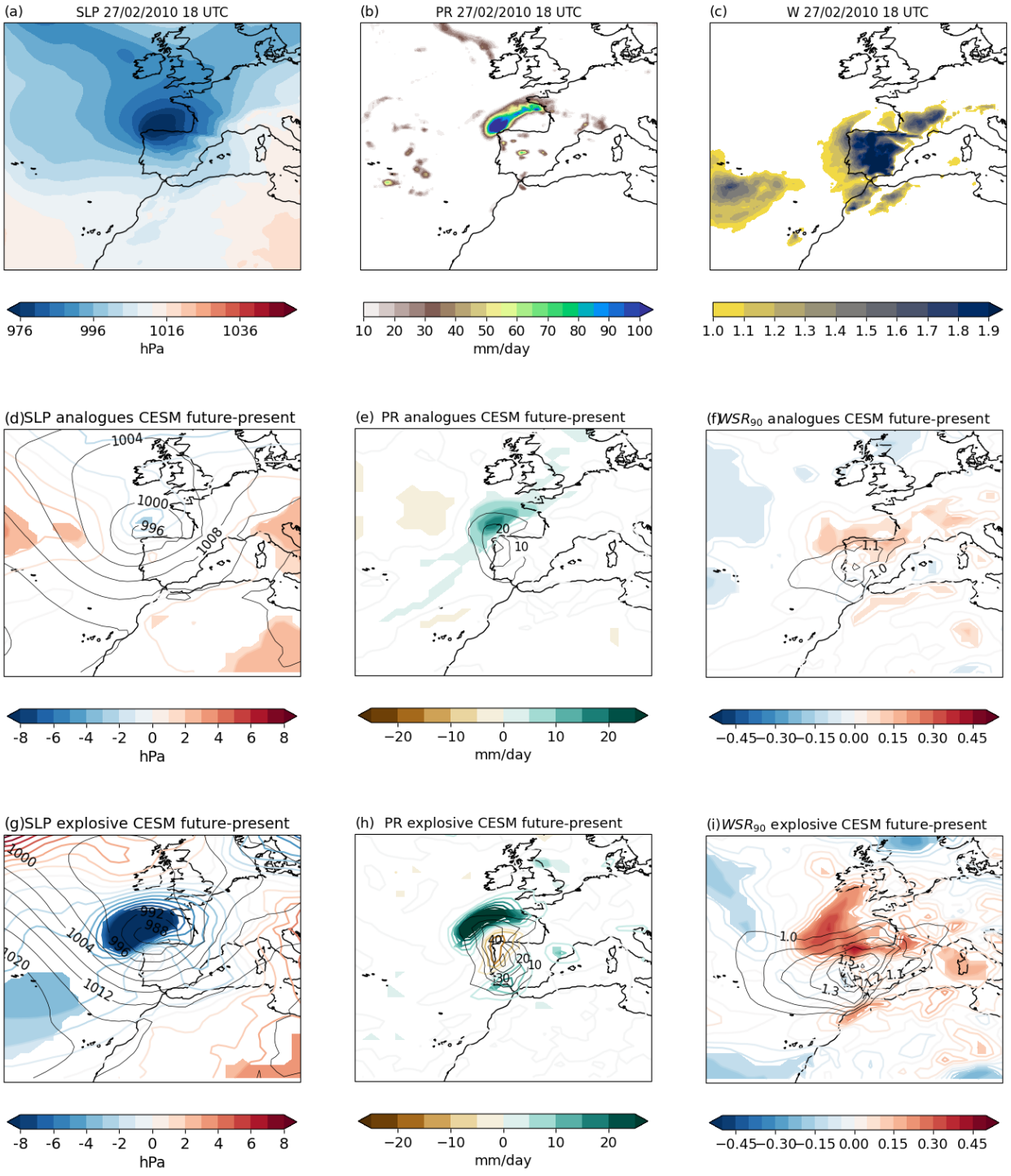

FIG. 17. Same as figure 9 but for **analogues of Xynthia**.

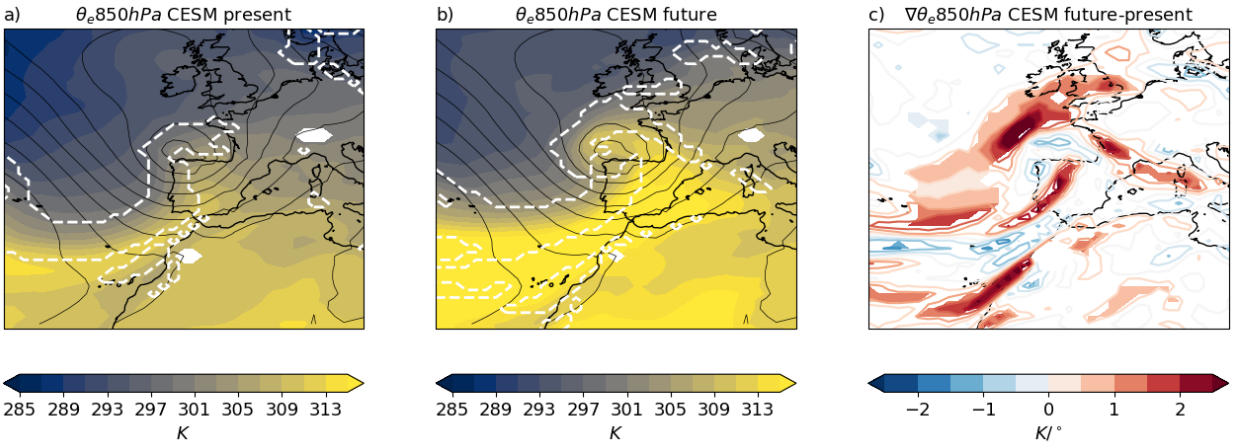

FIG. 18. Same as figure 10 but for storm **Xynthia**

Similar to storm Alex, Xynthia-like storms depict an extension downstream and southward of the jet stream in the future period (Fig. 19c). As previously discussed, this could lead to an increase in the vertical motion from the ageostrophic component of the wind and could be linked to the increase in precipitation and intensity of the storms. In addition, this position of the jet stream depicts a more advanced stage of the cyclone, and could be linked to the cyclonic relocation of the weather fronts.

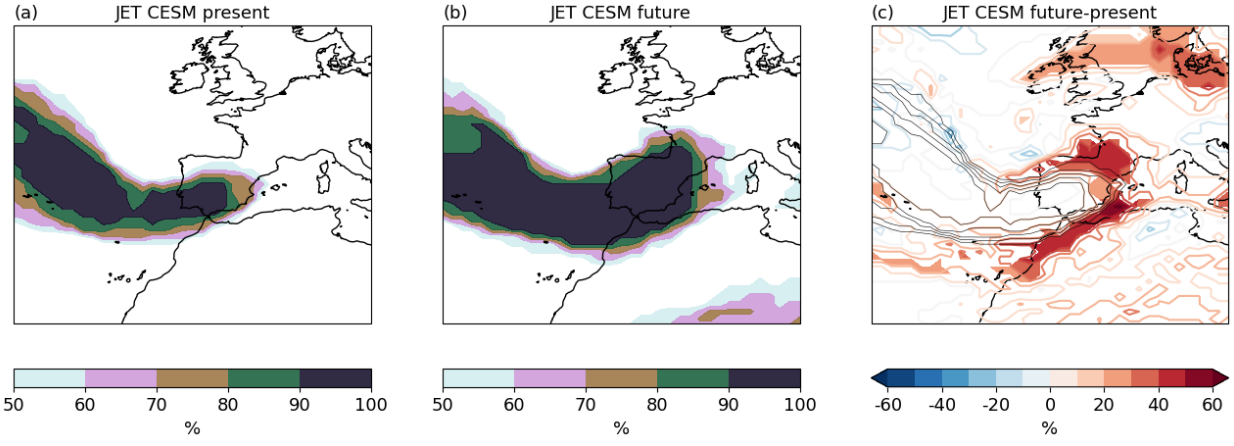

FIG. 19. Same as figure 11 but for storm **Xynthia**

Figure 20a depicts no change of the EGR in the region of its maximum, which means there are no changes in low-level baroclinicity 24 hours before the mature stage. Thus, changes assessed previously might be largely diabatically-driven. Regarding PRECC and PRECL (Fig. 20b,c)

spatial patterns, there is an overall increase in both types of precipitation. However, both show a tripolar pattern: a decrease in the core of the maximum precipitaiton area, and an increase in the southern and northern flanks. In the case of PRECL, this is linked to the cyclonic shift of the warm front and an intensification of both warm and cold fronts.

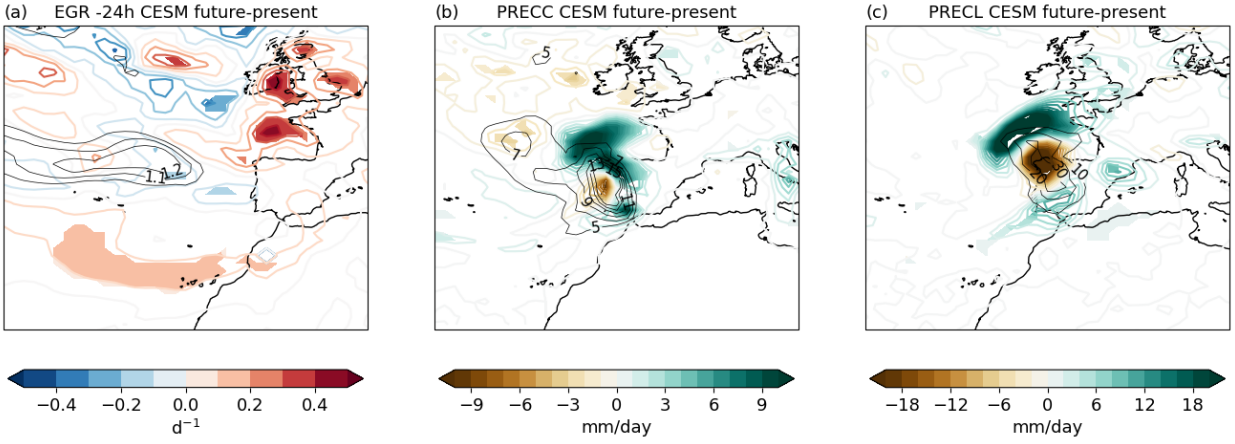

FIG. 20. Same as figure 12 but for storm **Xynthia**

7. Discussion and conclusions

We have conducted an analysis of three storms (Alex, Eunice, and Xynthia) under anthropogenic radiative forcing, using the CESM-Large Ensemble. We identified storms with a similar development stage to the three storms, and termed them *analogues*, in the present period (1991-2001) and in the future RCP8.5 period (2091-2100). We further selected those undergoing explosive cyclogenesis (*explosive analogues*). We found that the frequency and intensity of the analogue storms, as well as their associated meteorological hazards, will change in a future climate.

For storm Alex, a significant decrease in the number analogues has been observed, specially in autumn. However, there is an increase in the relative frequency of explosive analogues as well as in the normalized deepening rates. Both analogues and explosive analogues will be associated with overall higher precipitation and stronger wind speeds. The large-scale precipitation pattern of the explosive analogues and the weather front disposition suggest a cyclonic shift of the mature stage of the storms. There is a small increase in the baroclinicity in the future explosive analogues, which makes changes in their characteristics both baroclinically and diabatically driven. These factors suggest that explosive Alex-like storms will not be less frequent in a future climate. When

they occur, they will deepen more rapidly and be associated with higher precipitation and wind speeds, indicating that storms like Alex could be a greater meteorological hazard in the future.

For storm Eunice, rather than a change in the number of analogues, there is a seasonal shift towards more analogues in winter and fewer elsewhere. However, we found a significant increase in the number of analogues that undergo explosive cyclogenesis. The quality of both analogues and explosive analogues, computed using the Euclidean distance between the development stage of the storm and its analogues, also increases in a future climate. This means that analogues in the future climate are more similar in terms of tracks compared to the present, thereby increasing the likelihood of identifying more Eunice-like storms. Additionally, there will be an increase in precipitation rate and wind speed of the analogues and explosive analogues. These changes in the characteristics of explosive analogues are, at least partially, baroclinically-driven. Therefore, explosive Eunice-like storms will not only be more frequent but also more severe in a warmer climate.

We found it difficult to identify good analogues of storm Xynthia in both reanalysis and climate models. Hence, we can claim that storm Xynthia was an unusual event, and that a caveat of this study is the quality of its analogues. We observed a decrease in the number of analogues, specially in spring, but a slight increase in the relative frequency of explosive cyclogenesis. Xynthia-like storms are expected to have higher precipitation rates and wind speeds in a future climate. The explosive analogues depict an overall significant increase in precipitation and wind speed, with a cyclonic shift in their mature stage. Changes in the patterns of explosive analogues are likely to be largely diabatically-driven, as there is no change in low-level baroclinicity previous to the mature stage of the storms. Therefore, Xynthia-like storms are becoming less probable but more severe, especially those that are explosive, in a warmer climate. However, we acknowledge the low confidence in the results that arises from the limited quality and quantity of analogues available.

Changes in the number of analogues, including explosive ones, depend on the specific storm under consideration. Eunice-like explosive storms are expected to be more frequent, in line with previous studies that project a slight increase in explosive frequency close to the British Isles and on the North Sea (Seiler and Zwiers 2016; Zappa et al. 2013). The relative frequency of explosive storms like Alex and Xynthia is also expected to increase with respect to the non explosive storms. The increase in precipitation associated with storms in a future climate is consistent with other

studies (Hawcroft et al. 2018; Zhang and Colle 2017; Michaelis et al. 2017; Reale et al. 2022). For the explosive analogues of Alex and Xynthia, we found a similar precipitation changes to Sinclair et al. (2020). Sinclair et al. (2020) found, using aquaplanet simulations, a poleward displacement of the region of maximum precipitation, mainly due to changes in the large-scale precipitation pattern, in a future climate. There is less confidence in future projections regarding the dynamical intensity, such as wind speed, associated to the storms (Seneviratne et al. 2021; Catto et al. 2019). However, our study reveals that, across all the storms analysed, surface winds are expected to increase, specially for the explosive analogues and over land. For Eunice, the increase is located over the warm sector of the storms, as consistent with previous studies (Priestley and Catto 2022; Dolores-Tesillos et al. 2022). The drivers behind the changes in the pattern of the storms, whether they are baroclinically-driven or diabatically-driven, vary depending on the storm. However, as found by Dolores-Tesillos et al. (2022), Binder et al. (2023), and Joos et al. (2023), diabatic effects play a key role in increasing the wind speed, the deepening rates, and the intensity of the strongest storms. For the case of Xynthia, Ludwig et al. (2014) found that the storm intensification was mainly led by anomalously high sea surface temperatures and diabatic processes, and also suggested that Xynthia-like storms could be more frequent in a warmer climate. We note that we found no changes in low-level baroclinicity for Xynthia-like storms during the development stage. Hence, we suggest that diabatic processes contribute to the increase in wind and precipitation for Xynthia-like explosive storms in a future climate, as well as a relative increase of the explosive frequency, consistent with the prediction by Ludwig et al. (2014). In addition, Sinclair et al. (2020) found, using an aquaplanet model, that storms in a warmer climate are more diabatically-driven. To better understand the potential influence of diabatic effects on storm intensification, a comprehensive study on the role of warm conveyor belts in storm intensification (Binder et al. 2023) could be conducted. Our study thus identifies both similarities and differences when compared to previous research on various behaviors of extratropical and explosive storms in the North Atlantic under climate change. These findings not only emphasize the differences in regional changes but also suggest that storms may exhibit distinct behaviors compared to the overall changes, potentially yielding different responses to anthropogenic radiative forcing.

Our approach has limitations that should be acknowledged. First, our analysis is based on a single model, the CESM model version 1, which was chosen for its availability as a large ensemble

dataset of more than 100 members with 6-hourly data. While CESM has been shown to simulate the characteristics of storms fairly well (Dolores-Tesillos et al. 2022; Joos et al. 2023; Binder et al. 2023) and to have a spread due to internal variability comparable to the CMIP5 multi-model spread (Kay et al. 2015), it has certain biases that should be acknowledged. The model underestimates the number of cyclones, specially over the ocean, as well as the deepening rates of the most extreme cyclones. Moreover, our analysis is based on a small sample of cyclones, which may not fully represent the entire spectrum of cyclone behavior. While the model reproduces cyclone frequencies and deepening rates well within this limited sample, a multi-model study would provide a more comprehensive assessment of model uncertainty. Second, we use a single scenario, the worst-case scenario (RCP8.5), due to its availability. This scenario represents an extreme case assuming high greenhouse gas emissions throughout the 21st century. Although this extreme scenario proves valuable in detecting the anthropogenic radiative forcing signal, it may not encompass the entire range of future climate projections. Therefore, our findings may not be generalized to other scenarios. Future studies should explore the robustness of our results using multiple models and scenarios. Finally, we use a single tracking scheme. However, we filter out the weakest storms, and so the dependence on the tracking scheme is considered minor (Neu et al. 2013).

The analogues are considered recurrences in the atmospheric patterns of to the storms, and so our results can also be applied to the explosive analogues found in the ERA5 dataset, some of them being known high-impact storms in the region (Table A1). In conclusion, we found that all of the storms analyzed in this study are expected to become more severe and impactful with climate change. As suggested by Shepherd (2016), demonstrating that certain extreme events can occur again and result in even worse consequences with climate change, as shown in this study, can help advocate for investment in protective measures against hypothetical risks. Hence, these storms can serve as reference points for building resilience and preparing for future events.

Acknowledgments. This work was supported by the European Union's Horizon 2020 research and innovation programme under the Marie Sklodowska-Curie grant agreement N° 956396 (European weather extremes: drivers, predictability and impacts (EDIPI) ITN). The authors would like to express special thanks to H. Wernli and his Atmospheric Dynamics group at ETH Zurich, particularly M. Sprenger, M. Röthlisberger, H. Binder, J. Riboldi, and U. Beyerle, for their valuable discussions and assistance in accessing the CESM data.

Data availability statement. The ERA5 data are publicly available online at https://cds.climate.copernicus.eu/. We acknowledge the Atmospheric Dynamics and Climate Physics groups at ETH Zurich for providing access to CESM data.

APPENDIX

Alex			
Storm Angus	20 November 2016	United Kingdom, France	Also known as storm Nanette in France. The event left 2 fatalities and wind gusts up to 170 km/h (Sky News 2016; Met Office 2016; The telegraph 2016).
Storm Norberto	5 March 2020	France, Spain	Wind gusts around 100 km/h and up to 140 km/h were recorded (The European Forecaster 2021; AEMET 2021)
Storm Katie	28 March 2016	France, United Kingdom	The highest windgust recorded was 170 km/h in Isle of Wight (The European Forecaster 2021; AEMET 2021)
Eunice			
"Adolph Bermpohl" storm	23 February 1967	North Sea	The Adolph Bermpohl was a sea rescue cruiser on which its crew died due to the severity of the storm in the North Sea. Other boats also sank in the same storm (The Wreck Site 2017).
October storm	17 October 1967	Norway, Sweden	Hurricane-force winds of up to 144 km/h were recorded in some parts of southern Sweden (SMHI and Institute 2021).
Storm Capella	3 January 1976	Ireland, United Kingdom, Belgium, France, Denmark, Germany, Netherlands	Also known as Ruisbroek flood in Belgium. The storm resulted in severe wind damage across western and central Europe and coastal flooding. One of the strongest windgusts recorded during the event was 215 km/h at Lowther Hills (Met Office 1976). It left at least 82 fatalities (Berz 1988).
Burns' Day storm	25 January 1990	Ireland, United Kingdom, France, Belgium, Netherlands, Germany, Denmark	Also known as Storm Daria. Hurricane-force wind gust were recorded, such as 167 km/h at Abertporth (McCallum 1990) and 176 km/h at Pointe du Raz (Météo France 2019). The storm left at least 95 fatalities across Europe, being one of the deathliest storms in Europe (Météo France 2019).
Storm Oratia	30 October 2000	France, Germany, Netherlands and United Kingdom	Storm Oratia (Tora in Norway) (Extreme Wind Storms Catalogue n.d.) was probably the worst storm to hit United Kindgom after the Great Storm of 1987 (NASA Earth Observatory 2017). The storm brought heavy rainfall and strong winds to many areas of southern Britain, with wind gusts up to 150 km/h.
Storm Ulli	3 January 2012	United Kingdom, Ireland, Netherlands, Scandinavia	Storm Emil in Norway (The Nordic Page Norway n.d.). The damages were estimated at 0.2 billion USD (Koks and Haer 2020; Roberts et al. 2014b)
Storm Bronagh	21 September 2018	United Kingdom	Wind gusts up to 125 km/h recorded in the Isle of Wight (Met Office 2018).
Storm Christoph	21 January 2021	United Kingdom	The event was characterized by heavy precipitation above 100 mm. This was one of the wettest 3–day periods on record in the western and northwestern part of England and Wales (Met Office 2021).
Xynthia			
Storm Miguel	6 June 2019	Spain, France, Belgium, Luxemburg, Netherlands	The storm brought high winds and heavy precipitation to western Europe, with wind gusts up to 150 km/h (AEMET 2020; EUMETSAT 2019). It caused at least three deaths.

TABLE A1. Explosive analogues of each storm detected with ERA5, which are also known storms that had an impact across Europe. The first column corresponds to the storm name, the second column shows the date of minimum sea level pressure, the third column lists the regions affected, and the fourth column provides notes on some meaningful aspects.

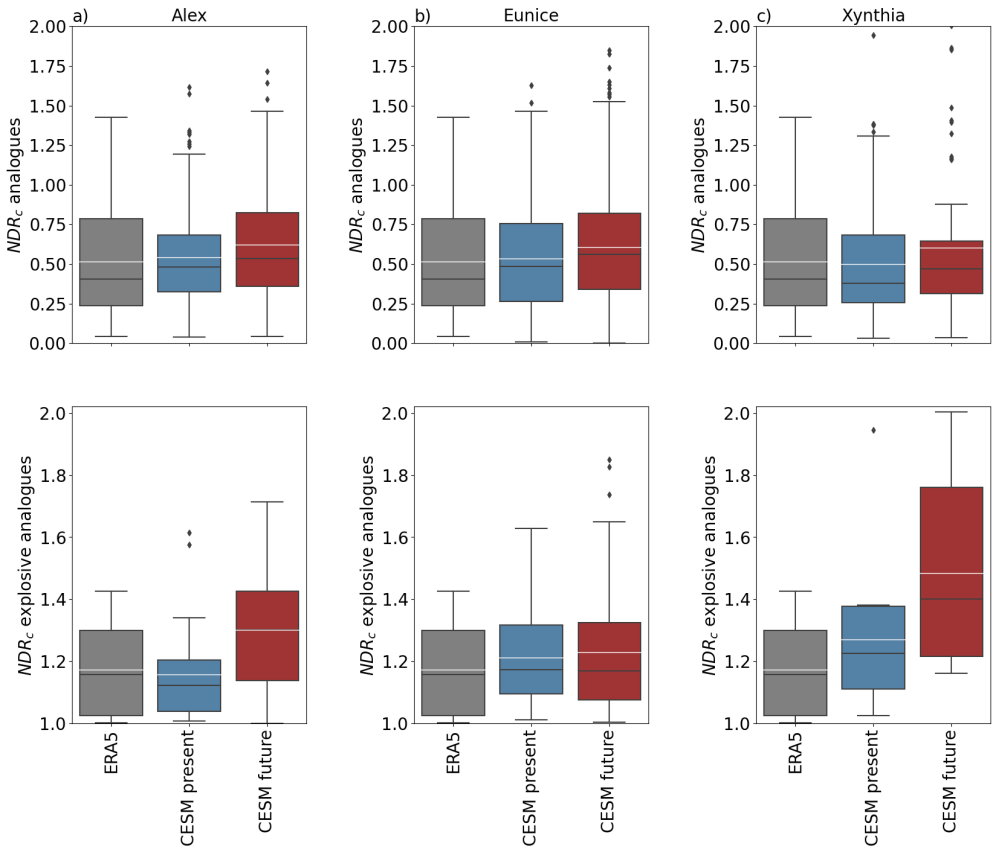

FIG. A1. Boxplot distributions of the Normalized Deepening Rates (NDR_c) of analogues (top row) and explosive analogues (bottom row) for Alex (a), Eunice (b), and Xynthia (c). Horizontal black lines represent the interquartile ranges of the distribution, while the white horizontal line indicates the mean values.

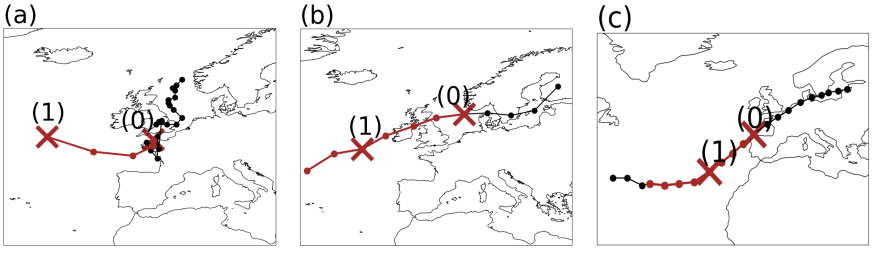

FIG. A2. 6–hourly tracks of storms Alex (a), Eunice (b), and Xynthia (c). (0) depicts the minimum sea level pressure point, and (1) the position of the storm 24 hours before (0). The brown line indicates when the storm underwent explosive cyclogenesis.

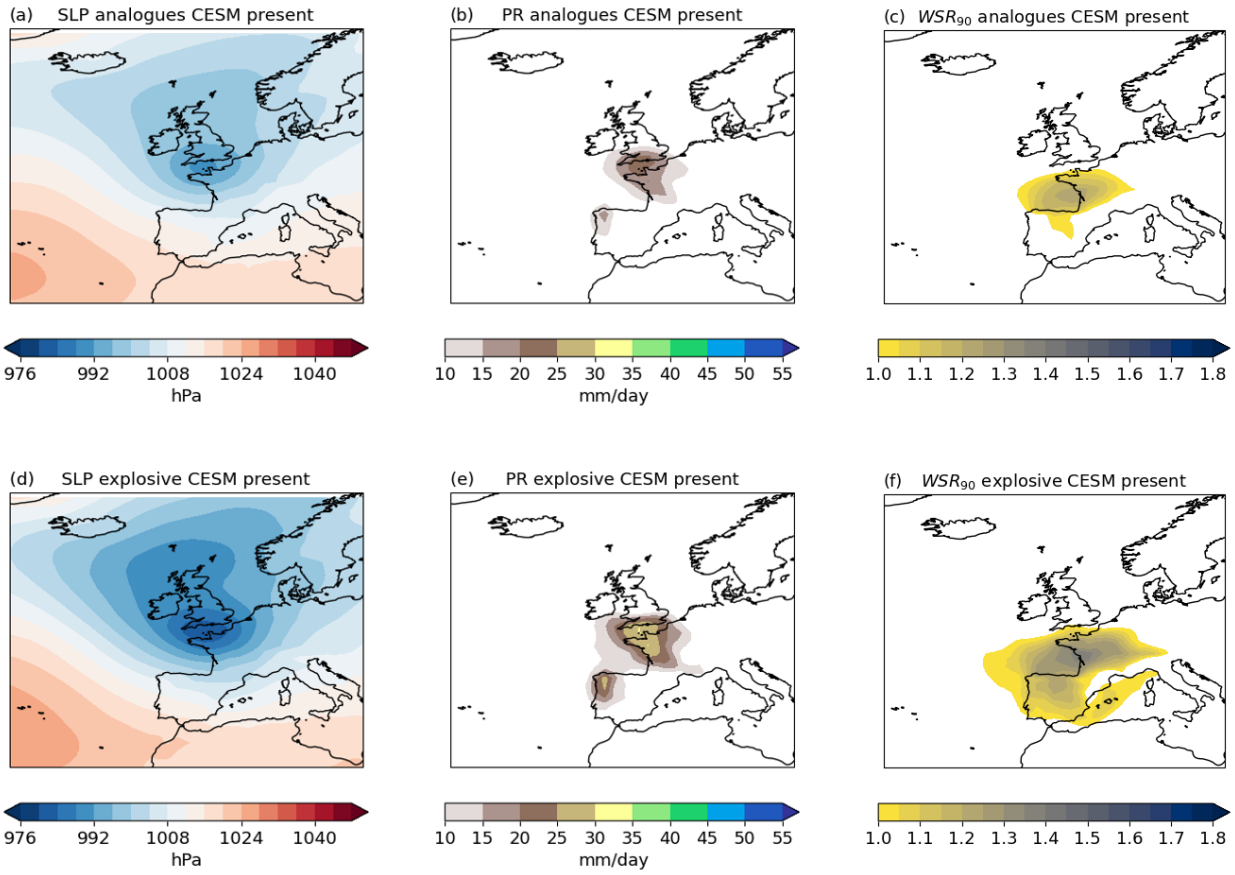

668 FIG. A3. Composites of the CESM present **analogues** and **explosive analogues** of **Alex** at their *time 0* dates
669 of (a,d) sea-level pressure, (b,e) hourly mean precipitation rate, and (c,f) hourly mean wind speed.

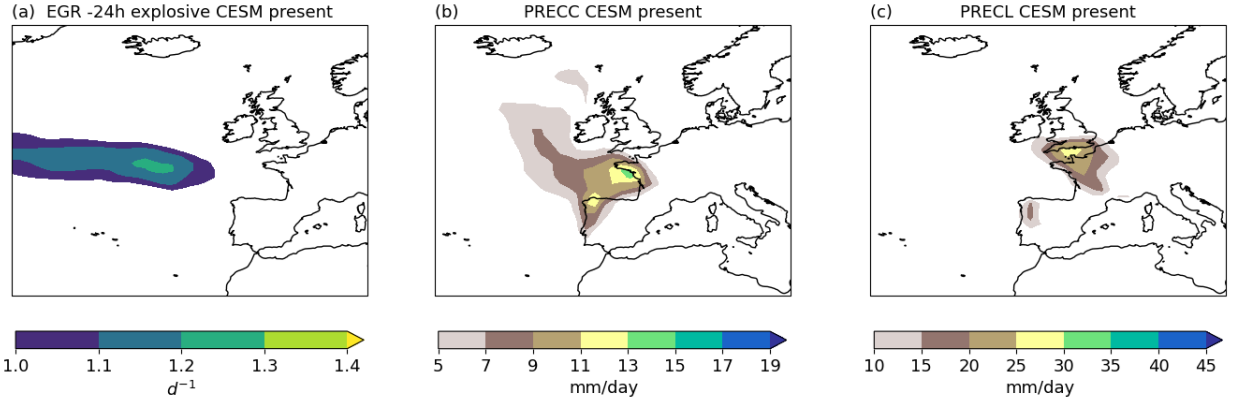

670 FIG. A4. Composites of the CESM present **explosive analogues** of **Alex** at their *time 0* dates of (a) eady
671 growth rate, (b) hourly mean convective precipitation, and (c) hourly mean large-scale precipitation rate.

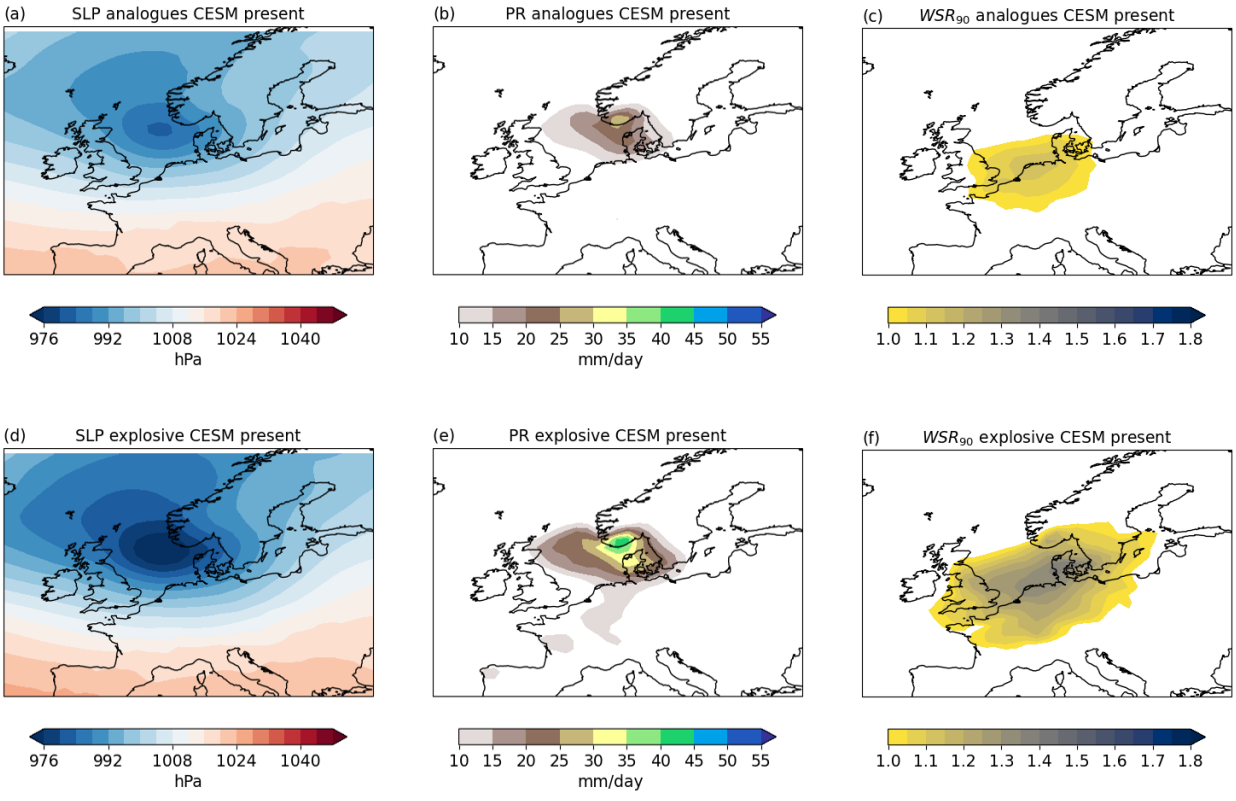

FIG. A5. Same as figure A3 but for **analogues of Eunice**.

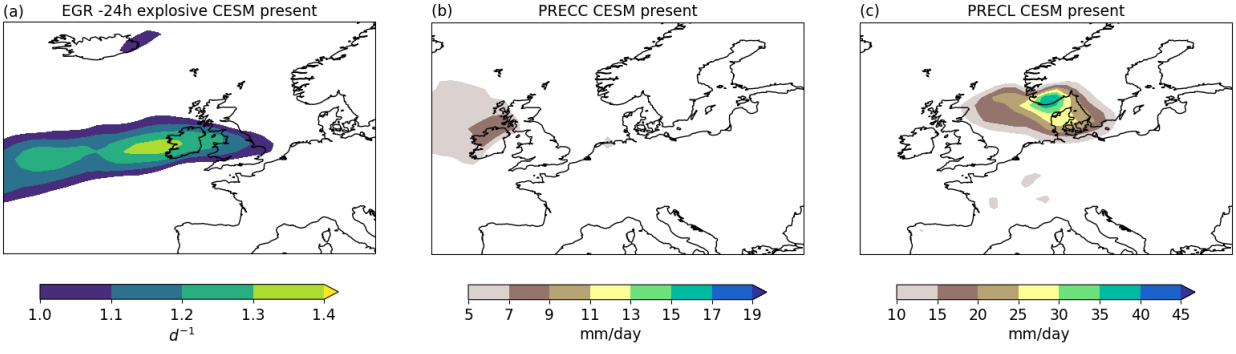

FIG. A6. Same as figure A4 but for **explosive analogues** of **Eunice**

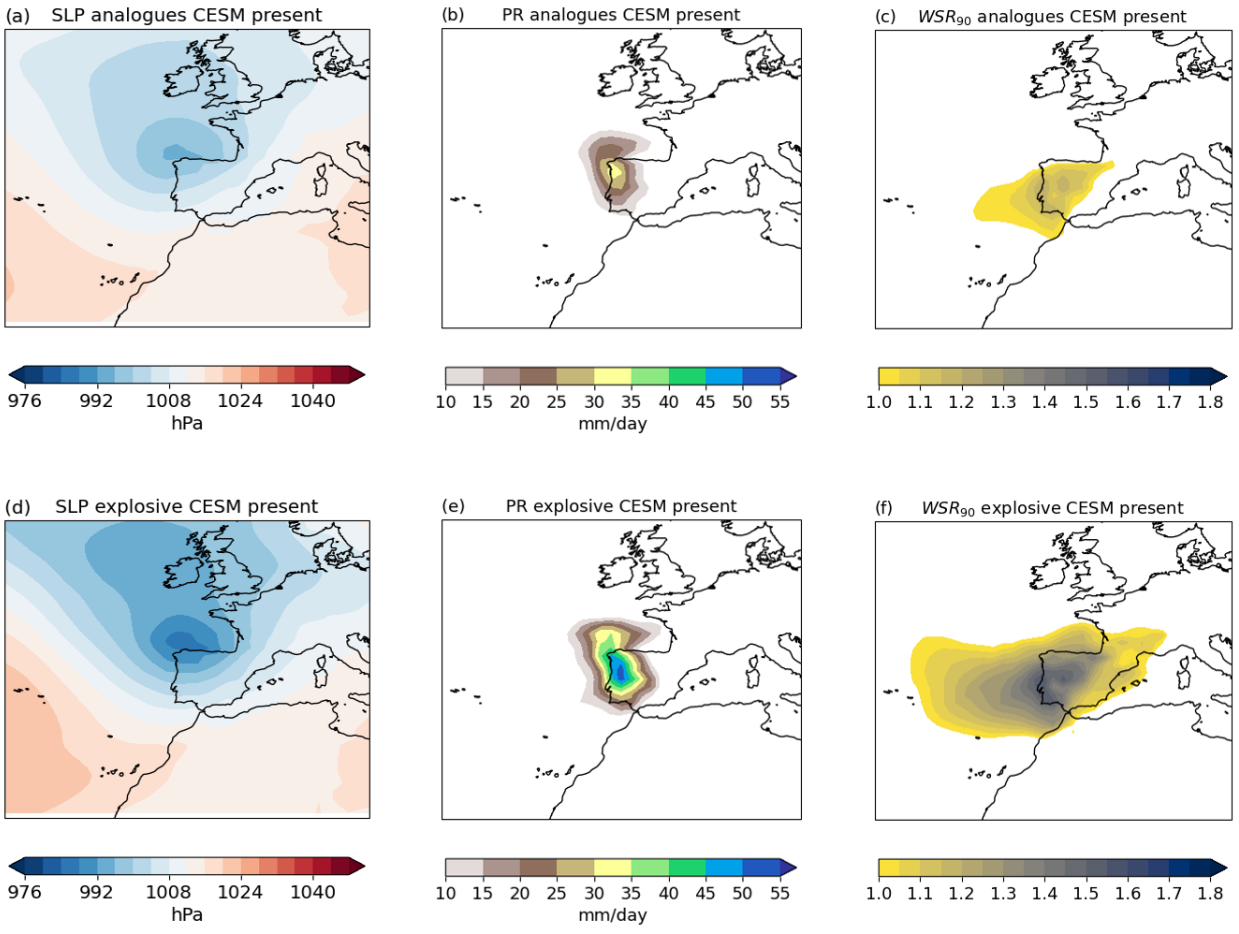

FIG. A7. Same as figure A3 but for **analogues of Xynthia**.

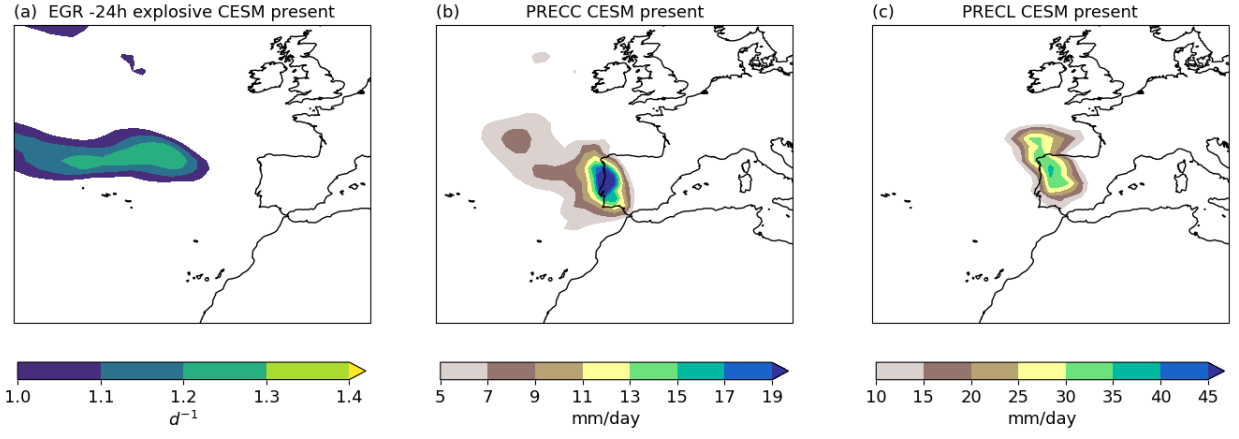

FIG. A8. Same as figure A4 but for **explosive analogues** of **Xynthia**

References

AEMET, 2020: Spanish state meteorological agency: Borrasca Miguel. Accessed: 2023-03-06, https://www.aemet.es/ca/conocermas/borrascas/2018-2019/estudios_e_impactos/miguel.

AEMET, 2021: Spanish state meteorological agency: Borrasca Norberto. Accessed: 2023-03-06, https://www.aemet.es/ca/conocermas/borrascas/2019-2020/estudios_e_impactos/norberto.

Allen, J. T., A. B. Pezza, and M. T. Black, 2010: Explosive cyclogenesis: A global climatology comparing multiple reanalyses. *Journal of Climate*, **23 (24)**, 6468–6484.

Anadolu Agency, 2022: Storm Eunice leaves 4 dead, over 400,000 homes without power in Poland. Accessed: 2023-01-11, https://www.aa.com.tr/en/europe/storm-eunice-leaves-4-dead-over-400-000-homes-without-power-in-poland/2507945.

Aon, 2020: Global Catastrophe Recap: October 2020. Available at: http://thoughtleadership.aon.com/documents/20201111_analytics-if-october-global-recap.pdf Accessed: October 202O.

BBC, 2022: Storm Eunice: Three people killed as strong winds sweep across UK. Accessed: 2023-01-11, https://www.bbc.com/news/uk-60439651.

Bertin, X., N. Bruneau, J.-F. Breilh, A. B. Fortunato, and M. Karpytchev, 2012: Importance of wave age and resonance in storm surges: The case xynthia, bay of biscay. *Ocean Modelling*, **42**, 16–30, https://doi.org/https://doi.org/10.1016/j.ocemod.2011.11.001, URL https://www.sciencedirect.com/science/article/pii/S1463500311001776.

Berz, G., 1988: List of major natural disasters, 1960–1987. *Natural Hazards*, **1 (1)**, 97–99.

Binder, H., H. Joos, M. Sprenger, and H. Wernli, 2023: Warm conveyor belts in present-day and future climate simulations–part 2: Role of potential vorticity production for cyclone intensification. *Weather and Climate Dynamics*, **4 (1)**, 19–37.

Brayshaw, D. J., B. Hoskins, , and M. Blackburn, 2009: The basic ingredients of the North Atlantic storm track. Part I: Land–sea contrast and orography. *Journal of Atmospheric Sciences*, **66**, 2539–2558, https://doi.org/0.1175/2009JAS3078.1.

Cattiaux, J., R. Vautard, C. Cassou, P. Yiou, V. Masson-Delmotte, and F. Codron, 2010: Winter 2010 in europe: A cold extreme in a warming climate. *Geophysical Research Letters*, **37 (20)**.

Catto, J. L., and Coauthors, 2019: The future of midlatitude cyclones. *Current Climate Change Reports*, **5**, 407–420.

Chadenas, C., A. Creach, and D. Mercier, 2014: The impact of storm xynthia in 2010 on coastal flood prevention policy in france. *Journal of Coastal Conservation*, **18 (5)**, 529–538.

Chauveau, E., and Coauthors, 2011: Xynthia: leçons d'une catastrophe. *Cybergeo: European Journal of Geography*.

Davolio, S., M. Vercellino, M. M. Miglietta, L. D. Pitura, S. Laviola, and V. Levizzani, 2022: The influence of an atmospheric river on a heavy precipitation event over the western alps. *Weather and Climate Extremes*, 100542.

Deser, C., A. Phillips, V. Bourdette, and H. Teng, 2012: Uncertainty in climate change projections: the role of internal variability. *Climate dynamics*, **38 (3)**, 527–546.

Deutsche Welle, 2022: Europe reckons with cost of Storm Zeynep. Accessed: 2023-01-11, https://www.dw.com/en/europe-reckons-with-cost-of-storm-zeynep/a-60823280.

Dolores-Tesillos, E., F. Teubler, and S. Pfahl, 2022: Future changes in north atlantic winter cyclones in cesm-le–part 1: Cyclone intensity, potential vorticity anomalies, and horizontal wind speed. *Weather and Climate Dynamics*, **3 (2)**, 429–448.

EUMETSAT, 2019: Storm Miguel batters parts of Europe. Accessed: 2023-03-06, https://www.eumetsat.int/storm-miguel-batters-parts-europe.

European State of the Climate, 2020: Storm Alex. Accessed: 2023-03-06, https://climate.copernicus.eu/esotc/2020/storm-alex.

Extreme Wind Storms Catalogue, n.d.: Oratia (Tora). Accessed: 2023-03-06, http://www.europeanwindstorms.org/cgi-bin/storms/storms.cgi?storm1=Oratia_Tora.

Faranda, D., S. Bourdin, M. Ginesta, M. Krouma, R. Noyelle, F. Pons, P. Yiou, and G. Messori, 2022: A climate-change attribution retrospective of some impactful weather extremes of 2021. *Weather and Climate Dynamics*, **3 (4)**, 1311–1340, https://doi.org/10.5194/wcd-3-1311-2022, URL https://wcd.copernicus.org/articles/3/1311/2022/.

Faranda, D., M. Ginesta, T. Alberti, E. Coppola, and M. Anzidei, 2023: Attributing venice acqua alta events to a changing climate and evaluating the efficacy of mose adaptation strategy. *npj Climate and Atmospheric Science*, **6 (1)**, 181.

Fink, A. H., T. Brücher, V. Ermert, A. Krüger, and J. G. Pinto, 2009: The european storm kyrill in january 2007: synoptic evolution, meteorological impacts and some considerations with respect to climate change. *Natural Hazards and Earth System Sciences*, **9 (2)**, 405–423, https://doi.org/10.5194/nhess-9-405-2009.

Fink, A. H., S. Pohle, J. G. Pinto, and P. Knippertz, 2012: Diagnosing the influence of diabatic processes on the explosive deepening of extratropical cyclones. *Geophysical Research Letters*, **39 (7)**.

Fischer, E. M., U. Beyerle, and R. Knutti, 2013: Robust spatially aggregated projections of climate extremes. *Nature Climate Change*, **3 (12)**, 1033–1038.

García-Pereda (NWC SAF/AEMET), J., 2010: Storm Xynthia. URL https://www.eumetsat.int/storm-xynthia.

Ginesta, M., P. Yiou, G. Messori, and D. Faranda, 2022: A methodology for attributing severe extratropical cyclones to climate change based on reanalysis data: the case study of storm alex 2020. *Climate Dynamics*, 1–25.

Harvey, B., P. Cook, L. Shaffrey, and R. Schiemann, 2020: The response of the northern hemisphere storm tracks and jet streams to climate change in the cmip3, cmip5, and cmip6 climate models. *Journal of Geophysical Research: Atmospheres*, **125 (23)**, e2020JD032 701.

Hawcroft, M., E. Walsh, K. Hodges, and G. Zappa, 2018: Significantly increased extreme precipitation expected in europe and north america from extratropical cyclones. *Environmental Research Letters*, **13 (12)**, 124 006, https://doi.org/10.1088/1748-9326/aaed59, URL https://doi.org/10.1088/1748-9326/aaed59.

Hawcroft, M. K., L. C. Shaffrey, K. I. Hodges, and H. F. Dacre, 2012: How much northern hemisphere precipitation is associated with extratropical cyclones? *Geophysical Research Letters*, **39 (24)**, https://doi.org/https://doi.org/10.1029/2012GL053866, URL https://agupubs.

onlinelibrary.wiley.com/doi/abs/10.1029/2012GL053866, https://agupubs.onlinelibrary.wiley.com/doi/pdf/10.1029/2012GL053866.

Hawkins, E., and R. Sutton, 2009: The potential to narrow uncertainty in regional climate predictions. *Bulletin of the American Meteorological Society*, **90 (8)**, 1095 – 1108, https://doi.org/https://doi.org/10.1175/2009BAMS2607.1, URL https://journals.ametsoc.org/view/journals/bams/90/8/2009bams2607_1.xml.

Hersbach, H., and Coauthors, 2020: The era5 global reanalysis. *Quarterly Journal of the Royal Meteorological Society*, **146 (730)**, 1999–2049, https://doi.org/https://doi.org/10.1002/qj.3803, URL https://rmets.onlinelibrary.wiley.com/doi/abs/10.1002/qj.3803, https://rmets.onlinelibrary.wiley.com/doi/pdf/10.1002/qj.3803.

Hurrell, J. W., and Coauthors, 2013: The community earth system model: a framework for collaborative research. *Bulletin of the American Meteorological Society*, **94 (9)**, 1339–1360.

Jansa, A., P. Alpert, A. Buzzi, and P. Arbogast, 2001: Medex, cyclones that produce high impact weather in the mediterranean. *Avalaible at http://medex. aemet. uib. es*.

Jézéquel, A., V. Dépoues, H. Guillemot, M. Trolliet, J.-P. Vanderlinden, and P. Yiou, 2018: Behind the veil of extreme event attribution. *Climatic Change*, **149**, 367–383.

Joos, H., M. Sprenger, H. Binder, U. Beyerle, and H. Wernli, 2023: Warm conveyor belts in present-day and future climate simulations-part 1: Climatology and impacts. *Weather and Climate Dynamics*, **4 (1)**, 133–155.

Kay, J. E., and Coauthors, 2015: The community earth system model (cesm) large ensemble project: A community resource for studying climate change in the presence of internal climate variability. *Bulletin of the American Meteorological Society*, **96 (8)**, 1333–1349.

Koch, P., H. Wernli, and H. C. Davies, 2006: An event-based jet-stream climatology and typology. *International Journal of Climatology: A Journal of the Royal Meteorological Society*, **26 (3)**, 283–301.

Koks, E., and T. Haer, 2020: A high-resolution wind damage model for europe. *Scientific Reports*, **10**, 6866, https://doi.org/10.1038/s41598-020-63580-w.

Kolen, B., R. Slomp, and S. Jonkman, 2013: The impacts of storm xynthia february 27–28, 2010 in france: lessons for flood risk management. *Journal of Flood Risk Management*, **6 (3)**, 261–278, https://doi.org/https://doi.org/10.1111/jfr3.12011, URL https://onlinelibrary.wiley.com/doi/abs/10.1111/jfr3.12011, https://onlinelibrary.wiley.com/doi/pdf/10.1111/jfr3.12011.

Lehmann, J., D. Coumou, K. Frieler, A. V. Eliseev, and A. Levermann, 2014: Future changes in extratropical storm tracks and baroclinicity under climate change. *Environmental Research Letters*, **9 (8)**, 084 002.

Liberato, M., J. Pinto, R. Trigo, P. Ludwig, P. Ordóñez, D. Yuen, and I. Trigo, 2013: Explosive development of winter storm xynthia over the subtropical north atlantic ocean. *Natural Hazards and Earth System Sciences*, **13 (9)**, 2239–2251.

Liberato, M. L., 2014: The 19 january 2013 windstorm over the north atlantic: large-scale dynamics and impacts on iberia. *Weather and Climate Extremes*, **5-6**, 16–28, https://doi.org/https://doi.org/10.1016/j.wace.2014.06.002, URL https://www.sciencedirect.com/science/article/pii/S2212094714000620.

Lim, E.-P., and I. Simmonds, 2002: Explosive cyclone development in the southern hemisphere and a comparison with northern hemisphere events. *Monthly Weather Review*, **130 (9)**, 2188–2209.

Liu, W. T., W. Tang, and X. Xie, 2008: Wind power distribution over the ocean. *Geophysical Research Letters*, **35 (13)**, https://doi.org/https://doi.org/10.1029/2008GL034172, URL https://agupubs.onlinelibrary.wiley.com/doi/abs/10.1029/2008GL034172, https://agupubs.onlinelibrary.wiley.com/doi/pdf/10.1029/2008GL034172.

Ludwig, P., J. G. Pinto, M. Reyers, and S. L. Gray, 2014: The role of anomalous sst and surface fluxes over the southeastern north atlantic in the explosive development of windstorm xynthia. *Quarterly Journal of the Royal Meteorological Society*, **140 (682)**, 1729–1741.

McCallum, E., 1990: The burns' day storm, 25 january 1990. *Weather*, **45 (5)**, 166–173.

Meinshausen, M., and Coauthors, 2011: The rcp greenhouse gas concentrations and their extensions from 1765 to 2300. *Climatic change*, **109 (1)**, 213–241.

Met Office, 1976: Monthly weather report: January 1976. Available at https://web.archive.org/web/20121023103203/http://www.metoffice.gov.uk/media/pdf/m/r/Jan1976.pdf.

Met Office, 2016: Storm angus. Available at https://www.metoffice.gov.uk/weather/warnings-and-advice/uk-storm-centre/storm-angus.

Met Office, 2018: Storm bronagh. Accessed: 2023-03-06, https://www.metoffice.gov.uk/weather/warnings-and-advice/uk-storm-centre/storm-bronagh.

Met Office, 2021: Storm Christoph 18 to 20 January 2021. Accessed: 2023-03-06, https://www.metoffice.gov.uk/binaries/content/assets/metofficegovuk/pdf/weather/learn-about/uk-past-events/interesting/2021/2021_01_storm_christoph.pdf.

Met Office, 2022: Storms dudley, eunice and franklin, february 2022. Available at: https://www.metoffice.gov.uk/binaries/content/assets/metofficegovuk/pdf/weather/learn-about/uk-past-events/interesting/2022/2022_01_storms_dudley_eunice_franklin_r1.pdf Accessed: March 2023.

Michaelis, A. C., J. Willison, G. M. Lackmann, and W. A. Robinson, 2017: Changes in winter north atlantic extratropical cyclones in high-resolution regional pseudo–global warming simulations. *Journal of Climate*, **30 (17)**, 6905 – 6925, https://doi.org/https://doi.org/10.1175/JCLI-D-16-0697.1, URL https://journals.ametsoc.org/view/journals/clim/30/17/jcli-d-16-0697.1.xml.

Météo France, 2019: Tempête DARIA du 25 janvier 1990. Available at http://tempetes.meteo.fr/IMG/anthemis_pdf/19900125.pdf.

Météo France, 2020: Tempête Alex: des intempéries exceptionnelles. Available at https://meteofrance.com/actualites-et-dossiers/climat/tempete-alex-des-intemperies-exceptionnelles.

NASA Earth Observatory, 2017: Superstorm Sweeps Over England. Accessed: 2023-03-06, https://wrecksite.eu/wreck.aspx?258019.

Neu, U., and Coauthors, 2013: Imilast: A community effort to intercompare extratropical cyclone detection and tracking algorithms. *Bulletin of the American Meteorological Society*, **94 (4)**, 529–547.

NL Times, 2022: Fourth death confirmed in Netherlands as Storm Eunice heads north. Accessed: 2023-01-11, https://nltimes.nl/2022/02/18/fourth-death-confirmed-netherlands-storm-eunice-heads-north.

Owen, L. E., J. L. Catto, D. B. Stephenson, and N. J. Dunstone, 2021: Compound precipitation and wind extremes over europe and their relationship to extratropical cyclones. *Weather and Climate Extremes*, **33**, 100 342, https://doi.org/https://doi.org/10.1016/j.wace.2021.100342, URL https://www.sciencedirect.com/science/article/pii/S2212094721000384.

Priestley, M. D. K., D. Ackerley, J. L. Catto, K. I. Hodges, R. E. McDonald, and R. W. Lee, 2020: An overview of the extratropical storm tracks in cmip6 historical simulations. *Journal of Climate*, **33 (15)**, 6315 – 6343, https://doi.org/10.1175/JCLI-D-19-0928.1, URL https://journals.ametsoc.org/view/journals/clim/33/15/JCLI-D-19-0928.1.xml.

Priestley, M. D. K., and J. L. Catto, 2022: Future changes in the extratropical storm tracks and cyclone intensity, wind speed, and structure. *Weather and Climate Dynamics*, **3 (1)**, 337–360, https://doi.org/10.5194/wcd-3-337-2022, URL https://wcd.copernicus.org/articles/3/337/2022/.

Rapella, L., D. Faranda, M. Gaetani, D. Philippe, and M. Ginesta, 2023: Climate change on extreme winds already affects off-shore wind power availability in europe. *Environmental Research Letters*.

Reale, M., M. L. Liberato, P. Lionello, J. G. Pinto, S. Salon, and S. Ulbrich, 2019: A global climatology of explosive cyclones using a multi-tracking approach. *Tellus A: Dynamic Meteorology and Oceanography*, **71 (1)**, 1611 340, https://doi.org/10.1080/16000870.2019.1611340.

Reale, M., and Coauthors, 2022: Future projections of mediterranean cyclone characteristics using the med-cordex ensemble of coupled regional climate system models. *Climate dynamics*, 1–24.

RMS, 2022: RMS estimates insured losses from windstorms Dudley and Eunice will likely range between 3.0 and 4.5 billion euro. Accessed: 2023-01-11, https://www.rms.com/newsroom/press-releases/press-detail/2022-03-01/rms-estimates-insured-losses-from-windstorms-dudley-and-eunice-will-likely-range-between-30-and-45

Roberts, J., and Coauthors, 2014a: The xws open access catalogue of extreme european windstorms from 1979 to 2012. *Natural Hazards and Earth System Sciences*, **14 (9)**, 2487–2501.

Roberts, J. F., and Coauthors, 2014b: The xws open access catalogue of extreme european windstorms from 1979 to 2012. *Natural Hazards and Earth System Sciences*, **14 (9)**, 2487–

2501, https://doi.org/10.5194/nhess-14-2487-2014, URL https://nhess.copernicus.org/articles/14/2487/2014/.

Roebber, P. J., 1984: Statistical analysis and updated climatology of explosive cyclones. *Monthly Weather Review*, **112**, 1577–1589, https://doi.org/https://doi.org/10.1175/1520-0493(1984)112⟨1577:SAAUCO⟩2.0.CO;2.

Röthlisberger, M., M. Sprenger, E. Flaounas, U. Beyerle, and H. Wernli, 2020: The substructure of extremely hot summers in the northern hemisphere. *Weather and Climate Dynamics*, **1 (1)**, 45–62, https://doi.org/10.5194/wcd-1-45-2020, URL https://wcd.copernicus.org/articles/1/45/2020/.

RTL Info, 2022: La tempête Eunice a balayé la Belgique: le bilan s'alourdit à 2 morts, les pompiers surchargés un peu partout dans le pays. Accessed: 2023-01-11, https://www.rtl.be/info/belgique/meteo/meteo-un-vent-tempetueux-attendu-ce-vendredi-voici-les-previsions-1357970.aspx.

Sanders, F., and J. R. Gyakum, 1980: Synoptic-dynamic climatology of the "bomb". *Monthly Weather Review*, **108**, 1589–1606, https://doi.org/https://doi.org/10.1175/1520-0493(1980)108⟨1589:SDCOT⟩2.0.CO;2.

Sansom, P. G., D. B. Stephenson, C. A. Ferro, G. Zappa, and L. Shaffrey, 2013: Simple uncertainty frameworks for selecting weighting schemes and interpreting multimodel ensemble climate change experiments. *Journal of Climate*, **26 (12)**, 4017–4037.

Schemm, S., 2023: Toward eliminating the decades-old "too zonal and too equatorward" storm-track bias in climate models. *Journal of Advances in Modeling Earth Systems*, **15 (2)**, e2022MS003 482, https://doi.org/https://doi.org/10.1029/2022MS003482, URL https://agupubs.onlinelibrary.wiley.com/doi/abs/10.1029/2022MS003482, e2022MS003482 2022MS003482, https://agupubs.onlinelibrary.wiley.com/doi/pdf/10.1029/2022MS003482.

Seiler, C., and F. W. Zwiers, 2016: How will climate change affect explosive cyclones in the extratropics of the northern hemisphere? *Climate Dynamics*, **46 (11)**, 3633–3644.

Seneviratne, S., and Coauthors, 2021: Weather and climate extreme events in a changing climate. In Climate Change 2021: The physical science basis. Contribution of Working Group I to the Sixth Assessment Report of the Intergovernmental Panel on Climate Change [Masson-Delmotte, V., P. Zhai, A. Pirani, S.L. Connors, C. Péan, S. Berger, N. Caud, Y. Chen, L. Goldfarb, M.I. Gomis,

M. Huang, K. Leitzell, E. Lonnoy, J.B.R. Matthews, T.K. Maycock, T. Waterfield, O. Yelekçi, R. Yu, and B. Zhou (eds.)]. Cambridge University Press. In Press. Cambridge University Press.

Shapiro, M. A., and D. Keyser, 1990: *Fronts, Jet Streams and the Tropopause*, 167–191. American Meteorological Society, Boston, MA, https://doi.org/10.1007/978-1-944970-33-8_10, URL https://doi.org/10.1007/978-1-944970-33-8_10.

Shaw, T. A., and Coauthors, 2016: Storm track processes and the opposing influences of climate change. *Nature Geosci*, **9**, 656–664, https://doi.org/https://doi.org/10.1038/ngeo2783.

Shepherd, T. G., 2016: A common framework for approaches to extreme event attribution. *Current Climate Change Reports*, **2**, 28–38.

Sinclair, M. R., 1995: A climatology of cyclogenesis for the southern hemisphere. *Monthly Weather Review*, **123 (6)**, 1601 – 1619, https://doi.org/10.1175/1520-0493(1995)123⟨1601:ACOCFT⟩2.0.CO;2, URL https://journals.ametsoc.org/view/journals/mwre/123/6/1520-0493_1995_123_1601_acocft_2_0_co_2.xml.

Sinclair, V. A., M. Rantanen, P. Haapanala, J. Räisänen, and H. Järvinen, 2020: The characteristics and structure of extra-tropical cyclones in a warmer climate. *Weather and Climate Dynamics*, **1 (1)**, 1–25, https://doi.org/10.5194/wcd-1-1-2020, URL https://wcd.copernicus.org/articles/1/1/2020/.

Sky News, 2016: Storm angus: Body found in search for pensioner after flood. Available at https://news.sky.com/story/woman-dies-after-folkestone-storm-angus-rescue-10667386.

SMHI, S. M., and H. Institute, 2021: Den svåra oktoberstormen 1967. Accessed: 2023-03-06, https://www.smhi.se/kunskapsbanken/meteorologi/stormar-i-sverige/enskilda-stormar-och-ovader/den-svara-oktoberstormen-1967-1.5744.

The European Forecaster, 2021: The European Forecaster Newsletter of the WGCEF N° 26 September 2021. Accessed: 2023-03-06, http://www.euroforecaster.org/newsletter26/full.pdf.

The Irish Times, 2022: Storm Eunice: Council worker dies in Wexford after being struck by falling tree. Accessed: 2023-01-11, https://www.irishtimes.com/news/ireland/irish-news/storm-eunice-council-worker-dies-in-wexford-after-being-struck-by-falling-tree-1.4805979.

The Nordic Page Norway, n.d.: "Emil" to hit southern norway. Available at https://www.tnp.no/norway/panorama/2601-34emil34-is-to-strike-southern-norway/.

The telegraph, 2016: UK weather: Woman dies after being winched from the sea as storm Angus battersBritain. Available at https://www.telegraph.co.uk/news/2016/11/21/uk-weather-heavy-rain-causes-flooding-wake-storm-angus/.

The Wreck Site, 2017: MV Adolph Bermpohl (+1967) . Accessed: 2023-03-06, https://wrecksite.eu/wreck.aspx?258019.

Trenberth, K. E., J. T. Fasullo, and T. G. Shepherd, 2015: Attribution of climate extreme events. *Nature Climate Change*, **5 (8)**, 725–730.

Uccellini, L. W., 1990: Processes contributing to the rapid development of extratropical cyclones. *Extratropical Cyclones: The Erik Palmén Memorial Volume*, 81–105.

Vinet, F., D. Lumbroso, S. Defossez, and L. Boissier, 2012: A comparative analysis of the loss of life during two recent floods in france: the sea surge caused by the storm xynthia and the flash flood in var. *Natural hazards*, **61 (3)**, 1179–1201.

Wallace, J. M., and P. V. Hobbs, 2006: 10 - climate dynamics. *Atmospheric Science (Second Edition)*, J. M. Wallace, and P. V. Hobbs, Eds., second edition ed., Academic Press, San Diego, 419–465, https://doi.org/https://doi.org/10.1016/B978-0-12-732951-2.50015-6, URL https://www.sciencedirect.com/science/article/pii/B9780127329512500156.

Wernli, H., and C. Schwierz, 2006: Surface cyclones in the era-40 dataset (1958–2001). part i: Novel identification method and global climatology. *Journal of the atmospheric sciences*, **63 (10)**, 2486–2507.

WMO, 2020: Mediterranean episode causes "unprecedented" rainfall. Available at https://public.wmo.int/en/media/news/mediterranean-episode-causes-unprecedented-rainfall.

Worlwide, A., 2010: European Winterstorm Xynthia. URL https://alert.air-worldwide.com/extratropical-cyclone/2010/european-winterstorm-xynthia/update-1/.

Yiou, P., 2014: Anawege: a weather generator based on analogues of atmospheric circulation. *Geoscientific Model Development*, **7 (2)**, 531–543.

Zappa, G., L. Shaffrey, K. Hodges, P. Sansom, and D. Stephenson, 2013: A multimodel assessment of future projections of north atlantic and european extratropical cyclones in the cmip5 climate models. *Journal of Climate*, **26**, 5846–5862, https://doi.org/10.1175/JCLI-D-12-00573.1.

Zhang, Z., and B. A. Colle, 2017: Changes in extratropical cyclone precipitation and associated processes during the twenty-first century over eastern north america and the western atlantic using a cyclone-relative approach. *Journal of Climate*, **30 (21)**, 8633 – 8656, https://doi.org/https://doi.org/10.1175/JCLI-D-16-0906.1, URL https://journals.ametsoc.org/view/journals/clim/30/21/jcli-d-16-0906.1.xml.